

Application of the Monte Carlo method with meshless random walk procedure to selected scalar elliptic problems

S. MILEWSKI

*Cracow University of Technology, Department of Civil Engineering,
Institute for Computational Civil Engineering, Warszawska 24, 31-155 Cracow,
Poland, e-mail: s.milewski@L5.pk.edu.pl*

THE COMBINED STOCHASTIC-DETERMINISTIC APPROACH, which may be applied to the numerical analysis of a wide range of scalar elliptic problems of civil engineering, is presented in this paper. It is based on the well-known Monte Carlo concept with a random walk procedure, in which series of random paths are constructed. Additionally, it incorporates selected features of the meshless finite difference method, especially star selection criteria and a local weighted function approximation. The approach leads to the explicit stochastic formula relating one unknown function value with all a-priori known data parameters. Therefore, it allows for a fast and effective estimation of the solution value at the selected point(s), without the necessity of generation of large systems of equations, combining all unknown values. In such a manner, the proposed approach develops and extends the original standard Monte Carlo one toward analysis of boundary value problems with more complex shape geometry, natural boundary conditions, non-homogeneous right-hand sides as well as anisotropic and non-linear material models.

The paper is illustrated with numerical results of selected elliptic problems, including a torsion problem of a prismatic bar, a stationary heat flow analysis with anisotropic and non-linear material functions, as well as an inverse heat problem. Moreover, the appropriate coupling with other deterministic methods (e.g., the finite element method) is considered.

Key words: Monte Carlo method, random walk procedure, meshless finite difference method, elliptic problems, method coupling, non-linear problems, inverse problems.

Copyright © 2019 by IPPT PAN, Warszawa

1. Introduction

ELLIPTIC PROBLEMS OF MECHANICS are usually investigated by means of methods of deterministic type. In these (hard-computing) methods, a problem domain (line in 1D, plane in 2D, surface in 3D) is discretized by a set of nodes and/or elements as well as degrees of freedom. Moreover, the approximation of the unknown function, as well as its derivatives, is required. Degrees of freedom constitute primary unknowns to the final system of algebraic equations, which are generated by means of appropriate techniques, depending on the method's nature and problem formulation (collocation, functional minimisation, variational

principle). The system of equations yields one unique solution (providing the well-posedness of a problem), corresponding to the stationary load case. Among those deterministic solution approaches, one may distinguish the finite difference method (FDM [1, 2]), finite element method (FEM, [3]), boundary element method (BEM, [4]) or a wide group of meshless methods (MM, [1, 5–8]).

However, stochastic (soft-computing) methods of analysis may be applied as well. Their characteristic feature is that they may take data randomness into account, thus leading to the entire family of solutions, out of which one has to select the optimal solution. Therefore, in most cases, the original elliptic boundary value problem has to be reformulated into a new one, namely the non-linear optimisation problem or a set of stochastic differential equations. These new problems may be investigated by means of various stochastic approaches, namely the Monte Carlo (MC, [9, 10, 11]) method, fuzzy sets (FS, [12]), artificial neural networks (ANN, [13]) or genetic and evolutionary algorithms (GA and EA, [14, 17, 15]). Nevertheless, auxiliary boundary value problems, producing the family of admissible solutions, are usually solved by means of standard deterministic methods. Therefore, numerous combinations of deterministic and stochastic methods exist, for instance the stochastic BEM tailored for piezoelectric problems [16] or the coupled FE-GA method for solution of inverse problems (e.g., static load determination [17], parameters identification [18], topology optimisation [15]). In this paper, the special attention is laid upon the Monte Carlo method with a random walk (RW) of a meshless type. Although it rather constitutes a stochastic approach, it incorporates selected features typical for deterministic meshless methods, especially the meshless finite difference method (MFDM, [1, 8, 19–22]).

The Monte Carlo idea (developed by S. ULAM and J. VON NEUMANN, [9, 10]) may be applied to variety of algebraic and differential problems in which the solution determination may be troublesome or even impossible using analytical and deterministic numerical tools. Although subsequent Monte Carlo methods vary, according to their applications, they all tend to follow a particular pattern, namely: definition of a domain of possible inputs; random generation of inputs on the basis of a probability distribution over the domain; performance of a deterministic computation on the inputs and, aggregation of the results. Eventually, the number of (relevantly defined) successful inputs, related to the number of all inputs and scaled by the dimensional quantity (length, area, volume, function value) allows for the estimation of the unknown solution, providing the number of inputs is large enough. Applications of this simple Monte Carlo concept may concern, for instance, eigenvalues estimation [23], solution of linear systems of equations [24–26] numerical integration in multidimensional spaces [27, 28] or numerical solution of differential equations [29–36, 38, 39] at the selected internal point(s) of a problem domain, which is the focal point of this research.

The oldest works on this last subject [29, 30, 31] focus on the purely stochastic estimation of the solution of the Laplace differential equation at any internal point of the rectangular grid of mutually perpendicular lines. Random sampling of inputs is based upon the so called *random walks*. A single random walk describes a path that consists of a succession of random steps on this rectangular grid. Each path starts at the same internal point of a domain (where solution of Laplace equation is unknown) and terminates at boundary points (where this solution is known from boundary conditions), building the net of *boundary indications* (or *boundary hits*). The probability of each random step depends only on the state attained in the previous step (*a Markov chain*). The total sum of all numbers of boundary indications, scaled by a known solution at boundary points and related to the entire number of all random walks, estimates the solution of the Laplace equation at this particular internal point. It has been proved [30, 11] that this estimation converges with the finite difference solution obtained on the same grid of points, providing the number of random walks is large enough (the Monte Carlo concept).

Random walks may be classified into several different types. In the simplest case, both move directions and a step size of each random step are pre-defined (e.g., in case the regular grid of points is used), leading to the fixed random walk [11, 29–31, 40]. However, a rectangular grid of points may lead to large discretization errors in the case of more complex geometries, including, for instance, curvilinear edges, voids, corners etc. Therefore, several other types of random walks were developed, for instance semi floating random walk (step size is fixed, though the move direction is not limited, [41, 42]), full floating random walk (step size is not preassigned and changes at each step whereas the move direction is not limited, [37, 40–42]) or a meshless random walk [11], considered here. Furthermore, a continuous random walk minimizing the solution error has been proposed [33, 43, 44] along with the self-adaptive, grid-free algorithm, with improved solution smoothness and its application to diffusion equations [34]. The state-of-the-art of the MC/RW approach, as well as its recent developments (up to date) may be found in [35, 38, 39, 45, 46].

Similar stochastic concepts were successfully applied in variety of methods based upon the reformulation of the original boundary value problem to integration problem of stochastic equations [47, 48], including the well-known Feynman–Kac formula [49, 50]. They may be interpreted as methods for the evaluation of functional integrals of a specified continuous form. However, their practical application is limited by the existence of the explicit closed form solution formula. The relevant numerical solution approach is based upon the stochastic approximation of these integrals [48], which incorporates both the Monte Carlo method and the random walk procedure.

The proposed meshless random walk procedure is based upon several features of the MFDm, which uses rather totally arbitrarily irregular clouds of

nodes, than structured meshes (sets of nodes and elements). Therefore, all modifications of the current discretization (e.g., nodes shifting, removal, adding) may be performed without any difficulties, much more effectively and faster than in the FEM. Since there is no nodes connectivity, the MFDM (and other meshless methods) work well with problems with complex geometries, moving boundary, concentrated forces, crack propagation. Moreover, a-priori refined meshes and clouds of nodes may be applied, due to the complexity of load functions. However, several principles of the original MC/RW approach have to be reformulated and extended. First of all, potential directions of each subsequent move have to be selected according to appropriate direction selection criteria. Moreover, selection probabilities may be determined by difference schemes generated by means of the moving weighted least squares approximation (MWLS, [51, 52, 1, 8, 22]) of the unknown function. Additionally, those probabilities as well as the final MC formula should take into account the material anisotropy, boundary conditions of mixed types as well as non-homogeneous right-hand sides (load intensity). In such a manner, the proposed meshless Monte Carlo method may be considered as the combined deterministic-stochastic approach. Its deterministic nature is reflected by the following features, namely

- it does not require any additional reformulation of the original boundary value problem into a stochastic one,
- it may be applied to complex geometries and elliptic problems in more general form, due to the lack of a mesh structure and nodes regularity requirements,
- it takes into account all a-priori given data (e.g., load parameters, material coefficients, domain dimensions),
- it may be coupled with any arbitrary methods of deterministic and stochastic types, for instance, coupling MC/RW with the FE framework for analysis of the same problem, though in several subdomains; in each subdomain, a different method (e.g., in accordance with accuracy requirements and geometry limitations) is applied separately, followed by an additional integral over a domain interface, enforcing a solution continuity.

On the other hand, in the random walk technique, both step size and move directions are variable instead of being fixed, thus effectively adapting to a local distribution of nodes, curvilinear geometry and an equation type. Moreover, the meshless Monte Carlo approach delivers an explicit relation of a stochastic type, relating the output (an unknown function) and the input data (e.g., load parameters) at any arbitrary point of the domain; therefore it is especially convenient in problems in which the function values have to be determined multiple times (e.g., non-linear problems, solved in incremental-iterative manner (e.g., by means of simple iteration method or the Newton–Raphson approach), non-stationary problems, inverse problems). Finally, it is a very simple and fast solution ap-

proach, especially when the high accuracy of a solution is not among the most important aspects (e.g., a preliminary estimation of a solution for forthcoming iterative procedures).

The paper is organized as follows. Section 2 evokes the classic original MC/RW approach for Laplace equations, on the rectangular grid of points. Section 3 recalls the most important aspects of the proposed MC with meshless RW, discussed in [11] in more detailed manner. Section 4 is devoted to MC/RW algorithms for torsion problem of a prismatic bar. In Section 5, stationary heat flow problems, with anisotropic material functions, are investigated. In Section 6, heat problems with a non-linear material function are taken into account. Section 8 deals with the MC/RW formulation for inverse heat problems. Eventually, Section 7 presents a method coupling on the domain partitioned into several disjoint subdomains. It has to be stressed that the application of the MC/RW to problems, discussed in the last three sections, is reported here for the first time ever. The paper is briefly concluded and directions of future work are mentioned.

2. Standard Monte Carlo method with fixed random walk technique

The following 2D Laplace equation is considered

$$(2.1) \quad \frac{\partial^2 F}{\partial x_1^2} + \frac{\partial^2 F}{\partial x_2^2} = 0 \quad \text{in } \Omega$$

with essential boundary conditions

$$(2.2) \quad F = \bar{F}(x_1, x_2) \quad \text{on } \partial\Omega,$$

where $\Omega = \{\mathbf{x} = (x_1, x_2)\} \in \mathfrak{R}^2$ is the problem domain, $\partial\Omega$ - its boundary, $F : (x_1, x_2) \in \Omega \rightarrow \mathfrak{R}$ is the unknown C^2 scalar function, with given values $\bar{F}(x_1, x_2)$ at every boundary point. Let us assume that the grid of mutually perpendicular, n_1 horizontal and n_2 vertical lines, was generated, forming a mesh $\Omega_h \subset \Omega$, consisting of $n = n_1 \times n_2$ regularly spaced points (see Fig. 1, in which white dots indicate internal nodes where random walk begins/proceeds, whereas red dots are boundary nodes, where random walk terminates). Function values F_k at those points ($k = 1, \dots, n$) constitute the set of unknowns, while values at all boundary nodes (located on $\partial\Omega_h = \Omega_h \cap \partial\Omega$) are known. The following stochastic procedure may be adopted, in case only one function value (e.g., at domain centre point) is to be determined in a relatively fast manner and with reasonable accuracy:

1. Initiate the subsequent random walk starting from the given internal node $\mathbf{x}_k = (x_{1(k)}, x_{2(k)})$, randomly selecting one of the fourth equally possible

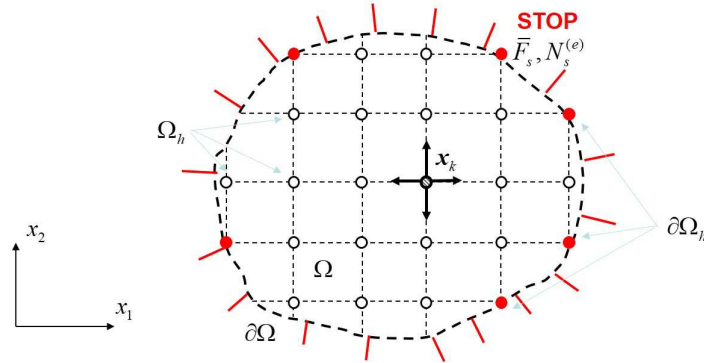


FIG. 1. Regular mesh of points with configuration of nodes (FD star) for a fixed random walk.

direction senses (north, east, south or west). Move to the closest neighbouring node, located in the selected direction (Fig. 1), and repeat the random walk from this new node as long as the first boundary node \mathbf{x}_r is reached. Evaluate the function value at this boundary node

$$(2.3) \quad \bar{F}_r = \bar{F}(\mathbf{x}_r)$$

and modify the number of its indications $N_r^{(e)}$ by one (we initialize all $N_r^{(e)}$ with zeros).

2. Return to the node of interest \mathbf{x}_k . Repeat the entire procedure described above until all N random walks are performed (N is the assumed total number of random walks).
3. Evaluate estimation of the function value F_k , according to the Monte Carlo concept (in which reaching the boundary node is treated as a successful input), by means of the simple formula

$$(2.4) \quad F_k \approx \frac{1}{N} \sum_r^{n^{(e)}} \bar{F}_r N_r^{(e)}$$

where $n^{(e)}$ denotes the number of all boundary nodes with essential boundary conditions (i.e., all boundary nodes in this case).

It has been proved [30] that this stochastic formula (2.4) corresponds to the finite difference (FD) solution, obtained for the considered regular mesh of nodes Ω_h . The proof is based upon the similarity of the stochastic system of equations to the one obtained by the standard FD method. In this manner,

the estimated function value (2.4) is convergent to the FD solution providing we assume the large number of random walks N . Therefore, N has the crucial influence on the accuracy of estimation (2.4). In the simplest cases, the Monte Carlo solution error may be upper-bounded by the non-linear function of N , namely

$$(2.5) \quad e = \|F_k - \bar{F}_k\| < \frac{1}{\sqrt{N}},$$

where \bar{F}_k is the exact solution of (2.1) at \mathbf{x}_k . This formula is valid providing there is no dimensionality dependence (i.e., a mesh size h has no influence on the solution estimation (2.4)). In other words, $\lim_{N \rightarrow \infty} F_k = \bar{F}_k$. It is important to notice that, unlike in deterministic methods, the estimate of the error (2.5) is not a strict error bound due to the fact that the random walks may not reach all boundary nodes with an appropriate frequency (especially for small N). Moreover, in case of differential equations in a more general form, discussed in the following sections, the relevant solution estimation becomes dependent on a mesh size h (constant for regular meshes, variable for irregular ones). In other words, $\lim_{N \rightarrow \infty} F_k = F_k^{(\text{FD})}$ and $\lim_{h \rightarrow 0} F_k^{(\text{FD})} = \bar{F}_k$, where $F_k^{(\text{FD})}$ is the corresponding finite difference (FD) solution at \mathbf{x}_k . Therefore, $\lim_{N \rightarrow \infty, h \rightarrow 0} F_k = \bar{F}_k$. The proper relation between N and h is usually determined a-posteriori [42, 11], by performing series of tests for various N with fixed h and controlling the stochastic error.

The standard MC method with a fixed RW technique exhibits numerous advantages, for instance, an existence of an explicit formula for an approximate solution, no curse of dimensionality, algorithm simplicity or low computational cost, which may be reflected in a potential parallelization of computations, since random walks may be performed independently from each other. However, it is limited to regular grids of points, second order differential equations of Laplace type (no heterogeneity in the right-hand side function), constant material coefficients as well as essential boundary conditions. However, the most important disadvantage seems to be an inability of considering problem domains with more complex geometries (e.g., with curvilinear edges and rounded corners, Fig. 1). Since one is able neither to generate a rectangular mesh with a reasonable mesh size nor to use local nodes refinements, the discretization error, resulting from $\partial\Omega_h \approx \partial\Omega$, would be very large in that case.

3. Monte Carlo method with meshless random walk technique

In order to overcome drawbacks and limitations of the standard MC method with a fixed random walk technique, the fundamental principles of the approach

have to be reformulated and extended. Those include: selection of potential move directions, selection of probabilities of selection of the following move as well as determination of the final MC formula. Since nodes may be distributed without any a-priori imposed structure (mesh regularity, element mesh, no mapping restrictions), it would be convenient to apply selected features typical for meshless methods (MM), especially the meshless FD method, which is one of the oldest MM, and therefore possibly the most developed one.

3.1. Selection of move directions

A random selection of four mutually perpendicular direction senses, with equal probabilities, which is natural for regular mesh, does not hold in case of irregular clouds of nodes. New direction selection criteria have to be carried out, taking advantage of the nodes' irregular distribution. Let us consider the determination problem of potential walk directions, starting from the central node (k) towards selected nodes numbered ($j(k)$), and $j(k) = 1, 2, \dots, m$. Both the total number of nodes ($m + 1$) in such a configuration (denoted as the MFD star or MFD stencil in MFD analysis), and their distribution should be assumed in such a manner that the resulting approximation scheme remains non-singular and non-ill-conditioned. Thus, m is usually larger than it is required from the order of differential operator (e.g., 6 nodes for 2D Laplace equation). The simplest criterion is based upon the distance from (k) to (j) nodes only. In more complex, 2D cross criterion [19, 21, 1, 8], the closest neighbourhood of node (k) is divided into four zones. Each of four semi-axes is assigned to one of these zones. A specified number of nodes (usually 2,3,4, depending on the derivatives' order), closest to the central node (point) is taken from every zone separately, thus the number of nodes in the MFD star is always constant. When comparing results

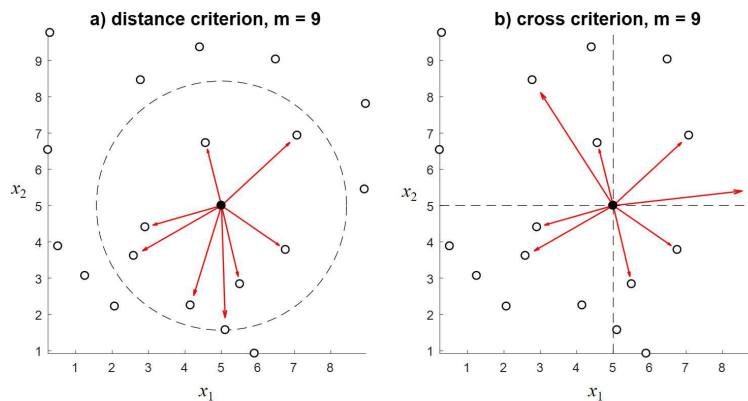


FIG. 2. Cloud of nodes and results of two main criteria for star selection.

obtained on the same cloud of nodes, for both a distance criterion (Fig. 2a) and a cross criterion (Fig. 2b), it may be observed that nodes are more well-balanced in the second case (i.e., the central node is located closer to the centre of gravity of selected nodes, which produces less approximation error). Consequently, this criterion was applied in all examples presented in this paper.

Regardless of the criterion applied, the resulting $[(m + 1) \times 2]$ matrix \mathbf{S}_k , representing a MFD star, contains numbers of nodes belonging to this star (first column) as well as distances between a central node and all other nodes (second column), usually sorted in an ascending order.

3.2. Selection of move direction probabilities

Consequently, equal probabilities of move direction, corresponding to the standard MC/RW approach, do not hold for heterogeneous distribution of move directions. Therefore, new rules have to be established, taking nodes irregularity into account. The most intuitive concept is based upon the inverse proportionality between a length measured between two nodes, located in a next move direction, and the probability of its selection. In other words, the longer this length is, the smaller the probability of its selection is. Such a concept may be implemented if a weighted version of moving least square (MLS) approximation is applied. The group of MLS methods is a typical approximation technique for variety of meshless methods. However, the MWLS (weighted MLS version, [51, 52, 1]), which is the most natural approximation technique for the MFD method, additionally uses singular weight functions which enforce interpolation properties of basis functions, despite its general approximation character (e.g., taking advantage of information overload). The MWLS constitutes a powerful tool, commonly applied to both generation of difference schemes [8, 22, 53] and for post-processing purposes (including methods other than meshless, for instance FEM, [54]).

Let us assume a configuration of nodes \mathbf{S}_k , with the central node \mathbf{x}_k , consisting of m other nodes $\mathbf{x}_{j(k)}$ (representing move directions from k to particular j). The local approximation F_k of a scalar function F , assigned to \mathbf{x}_k and at arbitrary \mathbf{x} , may be formulated as follows

$$(3.1) \quad F(\mathbf{x}) \approx F_k(\mathbf{x}_k, \mathbf{x}) = \mathbf{p}(\mathbf{x}_k, \mathbf{x}) \cdot \mathbf{D}_F(\mathbf{x}_k)$$

in which \mathbf{p} is a known $[1 \times s]$ vector of local interpolants $(\mathbf{x}_k - \mathbf{x})^l$, $l = 0, 1, \dots, p$, resulting from the Taylor series expansion of F at \mathbf{x} with respect to \mathbf{x}_k , whereas \mathbf{D}_F is an unknown $[s \times 1]$ vector of subsequent derivatives' values at \mathbf{x}_k , up to and including the approximation order p . Moreover, s is the number of Taylor series components, corresponding to p , for instance $s = 0.5(p + 1)(p + 2)$ in 2D case. It should be stressed that FEM and other meshless methods use equivalent

monomial notation [1, 5–7]. However, the Taylor series notation offers a simple and convenient interpretation of degrees of freedom (as local derivatives' values). Moreover, the approximation error may be evaluated without any difficulties, by the estimation of first neglected terms in (3.1).

Applying interpolation conditions at every node of \mathbf{S}_k leads to the over-determined system of $m + 1$ equations with s unknowns, namely

$$(3.2) \quad \mathbf{P} \cdot \mathbf{D}_F(\mathbf{x}_k) = \mathbf{F}_k$$

in which $\mathbf{P} = \mathbf{p}(\mathbf{x}_k, \mathbf{x}_{j(k)})$ is a $[(m + 1) \times s]$ matrix of local interpolants $(\mathbf{x}_k - \mathbf{x}_{j(k)})^l$, $j = 1, \dots, m + 1$, $l = 0, 1, \dots, p$, whereas \mathbf{F}_k is a $[(m + 1) \times 1]$ vector of degrees of freedom of F , for instance, function values at every node of \mathbf{S}_k . Afterwards, the weighted error function

$$(3.3) \quad I(\mathbf{x}_k) = (\mathbf{P} \cdot \mathbf{D}_F(\mathbf{x}_k) - \mathbf{F}_k)^T \cdot \mathbf{W}^2 \cdot (\mathbf{P} \cdot \mathbf{W}^2 \cdot \mathbf{D}_F(\mathbf{x}_k) - \mathbf{F}_k)$$

is determined, in which \mathbf{W} is a $[(m + 1) \times (m + 1)]$ diagonal weight matrix, with weights at its main diagonal, assigned to each node of \mathbf{S}_k , according to the formula

$$(3.4) \quad \omega_{j(k)} = \frac{1}{\|\mathbf{x}_k - \mathbf{x}_{j(k)}\|^{p+1} + \varepsilon}$$

in which ε is a positive and relatively small real number, preventing from a division by zero and corresponding to the assumed machine precision. Minimisation of (3.3), in the least square sense, yields the final formula for \mathbf{D}_F , namely

$$(3.5) \quad \mathbf{D}_F(\mathbf{x}_k) = \mathbf{M}_k \cdot \mathbf{F}_k, \quad \mathbf{M}_k = (\mathbf{P}^T \cdot \mathbf{W}^2 \cdot \mathbf{P})^{-1} \cdot \mathbf{P}^T \cdot \mathbf{W}^2.$$

Here, $\mathbf{M}_k = \mathbf{M}(\mathbf{x}_k)$ is a $[s \times (m + 1)]$ difference coefficients matrix. Values of all derivatives included in \mathbf{D}_F as well as values of any arbitrary differential operators of elliptic type (up to the assumed p -th order) may be composed by means of appropriate rows of \mathbf{M}_k , for instance

$$(3.6) \quad \begin{aligned} \left(\frac{\partial F}{\partial x_1} \right)_k &= \mathbf{M}_k^{<2>} \cdot \mathbf{F}_k = \sum_{j=0}^m M_{k2,j} \cdot F_{j(k)}, \\ \left(\frac{\partial F}{\partial x_2} \right)_k &= \mathbf{M}_k^{<3>} \cdot \mathbf{F}_k = \sum_{j=0}^m M_{k3,j} \cdot F_{j(k)} \end{aligned}$$

providing that $p \geq 1$ and

$$(3.7) \quad \begin{aligned} \left(\frac{\partial^2 F}{\partial x_1^2} \right)_k &= \mathbf{M}_k^{<4>} \cdot \mathbf{F}_k, & \left(\frac{\partial^2 F}{\partial x_1 x_2} \right)_k &= \mathbf{M}_k^{<5>} \cdot \mathbf{F}_k, \\ \left(\frac{\partial^2 F}{\partial x_2^2} \right)_k &= \mathbf{M}_k^{<6>} \cdot \mathbf{F}_k \end{aligned}$$

or

$$(3.8) \quad \left(\frac{\partial^2 F}{\partial x_1^2} \right)_k + \left(\frac{\partial^2 F}{\partial x_2^2} \right)_k = (\mathbf{M}_k^{<4>} + \mathbf{M}_k^{<6>}) \cdot \mathbf{F}_k = \sum_{j=0}^m (M_{k_{4,j}} + M_{k_{6,j}}) \cdot F_{j(k)}$$

corresponding to the Laplace operator in (2.1), providing that $p \geq 2$, etcetera. Here, $\mathbf{M}_k^{<i>}$ denotes the i -th row of \mathbf{M}_k ($i = 1, 2, \dots, s$).

Eventually, selection probabilities may be derived from approximation schemes (3.6)÷(3.8), dependently on the equation type, by rearranging terms in order to have an explicit formula for the central value (i.e., a function value at \mathbf{x}_k). For instance, for the Laplace operator (3.8), one has

$$(3.9) \quad F_k \sim - \frac{\sum_{j=1}^m (M_{k_{4,j}} + M_{k_{6,j}}) \cdot F_{j(k)}}{M_{k_{4,0}} + M_{k_{6,0}}}$$

whereas selection probabilities p_j are multipliers of $F_{j(k)}$, namely

$$(3.10) \quad p_j = - \frac{M_{k_{4,j}} + M_{k_{6,j}}}{M_{k_{4,0}} + M_{k_{6,0}}}, \quad j = 1, 2, \dots, m.$$

It should be noted that the total sum of all probabilities equals one ($\sum_{j=1}^m p_j = 1$), which is typical for elliptic difference operators. Therefore, selection of one of possible m directions, determined by \mathbf{S}_k , is a certain event.

3.3. The final Monte Carlo formula

Once potential directions of a next move (determined by \mathbf{S}_k) and corresponding selection probabilities (3.10) are known, general principles of a random walk procedure remain unmodified. The path of a particular random walk is generated as long as the first boundary node is reached, at which the solution value is given. As a consequence, not all boundary nodes terminate a random walk, since there may be natural boundary conditions posed, for which boundary derivatives are given, instead of a solution itself. Moreover, one has to build relevant statistics of indication numbers of all nodes reached along the path. It is required from the point of view of the final MC formula, which may be considered as a stochastic approximation of all a-priori known material and load parameters. Detailed formulas are given in the following sections, devoted to selected direct and inverse, linear and non-linear elliptic problems of mechanics.

4. Torsion problem of a prismatic bar

4.1. Problem formulation

The following mechanical problem is considered: find shear stress components τ_{x_1} and τ_{x_2} , generated on the cross-section of a long prismatic bar, clamped

at one end, subjected to a pure torsional load, given by a torsional angle θ . Assume linearly elastic material, represented by the Kirchhoff modulus G . The appropriate mathematical formulation is as follows: find such a function $F \in C^2$ which satisfies the following Poisson elliptic equation

$$(4.1) \quad \frac{\partial^2 F}{\partial x_1^2} + \frac{\partial^2 F}{\partial x_2^2} = -2G\theta \quad \text{in } \Omega$$

with essential homogeneous boundary conditions

$$(4.2) \quad F = 0 \quad \text{on } \partial\Omega.$$

Here, the 2D problem domain Ω represents the considered cross-section and F is a scalar Prandtl function whose derivatives yield stress components as well as the total average stress, namely

$$(4.3) \quad \tau_{x_1} = \frac{\partial F}{\partial x_2}, \quad \tau_{x_2} = -\frac{\partial F}{\partial x_1}, \quad \tau = \sqrt{\tau_{x_1}^2 + \tau_{x_2}^2}.$$

4.2. Computational model

Let us assume that the arbitrarily irregular cloud of nodes $\Omega_h \subset \Omega$ has been generated. The total number of nodes n may be decomposed as $n = n^{(e)} + n^{(i)}$, where $n^{(e)}$ is the number of boundary nodes (with an given function value equal 0), whereas $n^{(i)}$ is the number of internal nodes (with an unknown function value). Therefore, the Monte Carlo formula may be applied to any k -th internal node ($k = 1, 2, \dots, n^{(i)}$), with assigned star \mathbf{S}_k , consisting of m potential directions of a next move, determined by means of a cross criterion. The MWLS approximation allows for the determination of a difference coefficient matrix \mathbf{M}_k .

Applying a collocation technique (i.e., fulfillment of a difference equation at node) produces the following relation

$$(4.4) \quad \sum_{j=0}^m (M_{k_4,j} + M_{k_6,j}) \cdot F_{j(k)} = -2G\theta$$

at internal nodes, which yields selection probabilities in accordance with (3.10) and the additional right-hand side component, namely

$$(4.5) \quad F_k = -\frac{\sum_{j=1}^m (M_{k_4,j} + M_{k_6,j}) \cdot F_{j(k)}}{M_{k_4,0} + M_{k_6,0}} - \frac{2G\theta}{M_{k_4,0} + M_{k_6,0}} \\ = \sum_{j=1}^m p_j \cdot F_{j(k)} - \frac{2G\theta}{M_{k_4,0} + M_{k_6,0}}$$

Furthermore, the final explicit formula for F_k may be found after summation of indicators ($N_k^{(i)}$) of right-hand values (constant here), reached along all N random paths as well as by applying the Monte Carlo estimation of probabilities ($p_k \approx N_k^{(i)}/N$), namely

$$(4.6) \quad \begin{cases} F_k \approx -\frac{2G\theta}{N} \sum_k^{n^{(i)}} \frac{N_k^{(i)}}{M_{k_{4,0}} + M_{k_{6,0}}}, & k = 1, 2, \dots, n^{(i)}, \\ F_r = 0, & r = 1, 2, \dots, n^{(e)}. \end{cases}$$

Three situations may be distinguished, namely

1. The Prandtl function value is required at one point (node) only; in this case, the formula (4.6) is applied only once.
2. Shear stress components (4.3) are required at one point (node) only; in this case, the formula (4.6) is applied m times ($m \ll n$), for each node of a star, assigned to this point. Moreover, stress components (4.3) are computed by means of numerical differentiation technique, namely using the MWLS difference formulas from (3.6).
3. The Prandtl function values as well as shear stress components are required at every cloud node; in this case, the formula (4.6) is applied for all n nodes, separately.

It may be noted here that the simplified error estimation (2.5) may no longer hold, as the function value in (4.6) depends on both the number of random walks N and the cloud nodes dimension parameters, hidden inside difference coefficients ($M_{k_{4,0}}$ and $M_{k_{6,0}}$). However, (2.5) may still be applied in order to examine the convergence rate of (4.6) in terms of N .

4.3. Numerical examples

Two cross-section shapes are investigated, namely the simple rectangular one and the L-shape domain. Both geometric shapes are presented in Fig. 3, along with applied irregular clouds with $n = 100$ and $n = 183$ nodes, respectively. The following data was assumed: $G = 80$ GPa, $\theta = \pi/4$ and $m = 9$. First, one function value F , at one selected node for each domain, indicated in Fig. 3 ($\mathbf{x}_k = [0.46447, 0.53659]$ and $\mathbf{x}_k = [1.1309, 1.6472]$, respectively), was determined, on the set of increasing number of random walks (N changes from $N_{initial} = 20$, by $\Delta N = 200$, to $N_{final} = 10000$). For each fixed random walk number, the relative solution error was evaluated

$$(4.7) \quad e_N = \frac{|F_k - \bar{F}_k|}{|\bar{F}_k|}$$

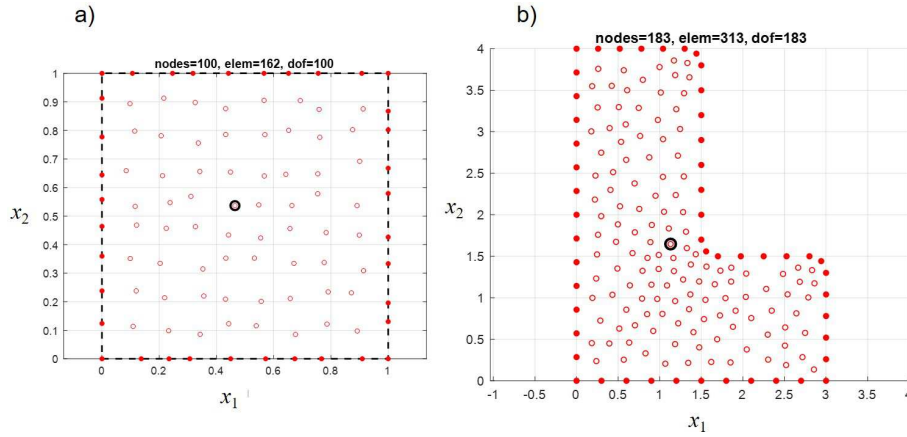


FIG. 3. Cross-section domains applied for a torsional problem: a) rectangular cross-section, b) L-Shape cross-section, with irregular distribution of nodes (100 and 183, respectively).

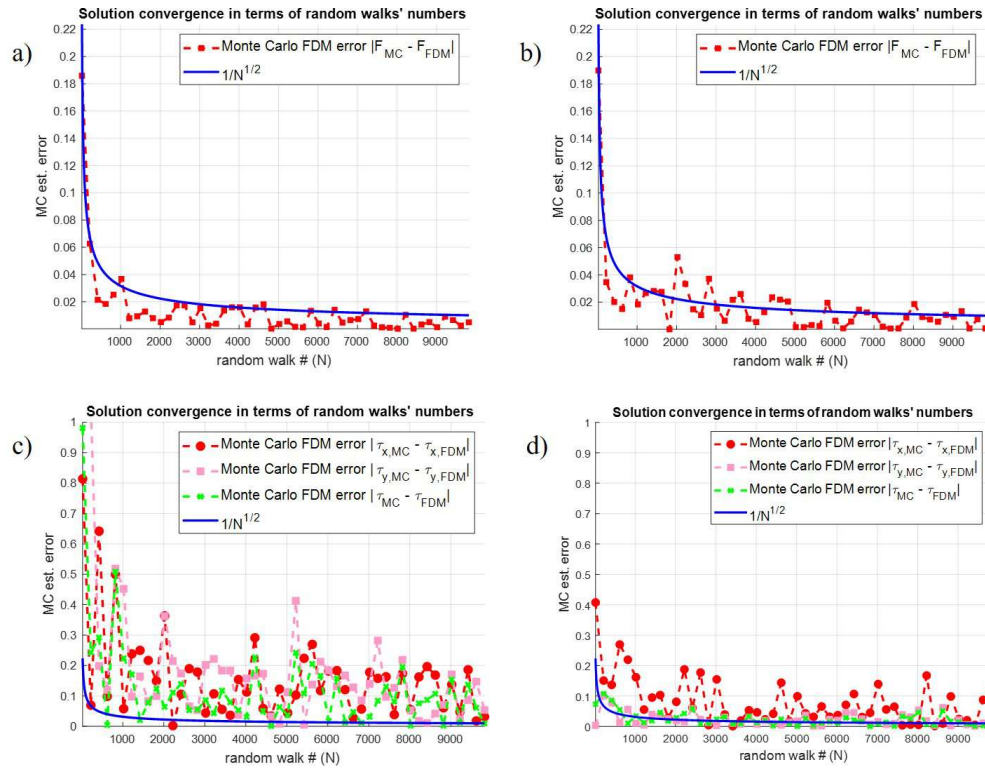


FIG. 4. Results of N -convergence study for a torsional problem a) Prandtl function N -convergence for the rectangular cross-section, b) Prandtl function N -convergence for the L-shape cross-section, c) stress components N -convergence for the rectangular cross-section, d) stress components N -convergence for the L-shape cross-section.

where \bar{F}_k is the high quality reference solution (here: the FD solution, corresponding to (4.1) and obtained on one rank denser clouds of 246 and 312 nodes, respectively). Error distribution is presented in Fig. 4a,b, in the form of N -convergence graphs, for both domains separately. The simple error estimation (2.5) is plotted as well, for comparison purposes.

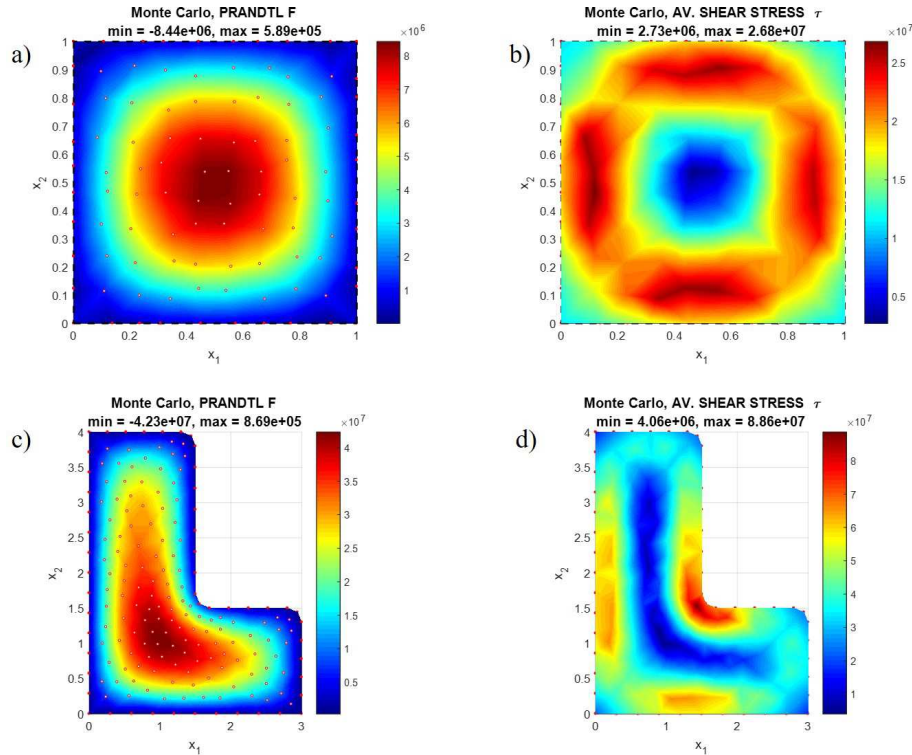


FIG. 5. Results of MC method applied for the entire cloud of nodes with $N = 1000$
 a) Prandtl function for the rectangular cross-section, b) average stress for the rectangular cross-section, c) Prandtl function for the L-shape cross-section, d) average stress for the L-shape cross-section.

Comparison of computational times t , required for the determination of one unknown value for the considered L-shape domain, for MFD and meshless MC methods separately, is presented in Fig. 6a, with respect to the number of nodes n in the cloud (for the fixed $N = 1000$). The total computational time for the FD analysis includes the dynamic allocation of the coefficient matrix and right-hand side vector, generation of approximation schemes and equations, fulfillment of relevant matrix rows and vector elements, the solution of system of equations (by means of optimally selected elimination method) as well as post-processing of results, whereas for the MC analysis, selection probabilities are computed

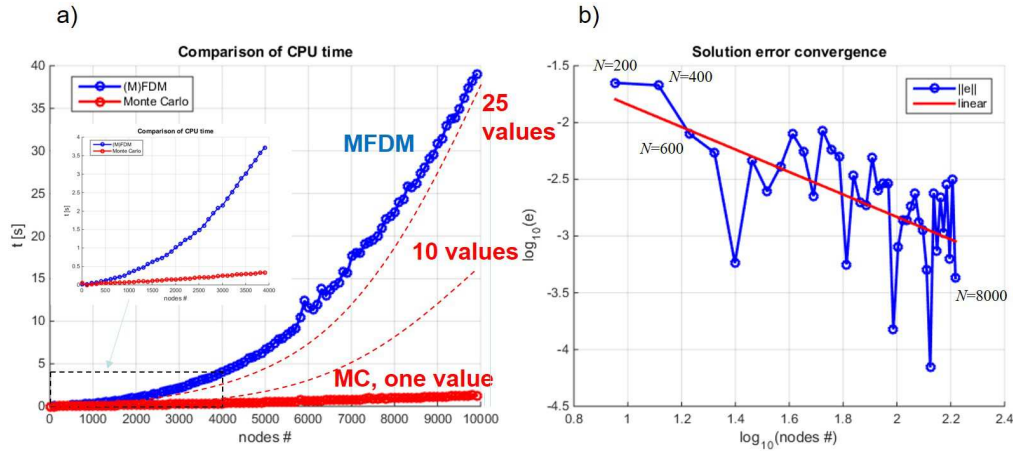


FIG. 6. Results for L-shape: comparison of computational time with respect to the number of nodes, for MFDM and MC methods (a) and results of h -convergence test (b).

along with the construction of random walks as well as application of the final MC formula. All computations were performed in Matlab R2014b, using 8 GB RAM as well as 1.80 GHz processor. Although Matlab is rather a slow high-level programming language (as the majority of its function bodies is loaded from the disc files), the key issues here is the difference and the improvement rate between FD and MC methods. Obviously, for each cloud of nodes, the MC formula (4.6) has to be applied only once, while the full system of FD equations has to be generated and solved. It may be observed that the MC curve $t = t(n)$ increases incomparably slower than the corresponding MFDM one. In case of larger number of unknown values (e.g., for shear stress evaluation), the MC curve may be scaled by this number (since all values may be computed separately), unless the appropriate parallelization of computations is performed (e.g., using many processors, with one processor for each unknown value). On the other hand, the MC method becomes ineffective, providing the number of unknown values is large (here, 25 unknown values on the cloud with $n = 10000$ nodes, computed by the MC method, require as much time as the generation and solution of the system of FD equations).

As it has been mentioned in the previous section, the solution error, caused by the MC solution estimation (4.6), is affected by both the number of random walks (N) and the discretization modulus (included in MWLS coefficients). The simple h -convergence test, performed for L-shape domain (see Fig. 6b, with numerical results and their linear regression), clearly shows that the stochastic type of error prevails over the discretization error. Fixing N and increasing n only would lead to no convergence at all. However, modifying both N and n in the same time may

lead to the reasonable convergence rate, though with no monotonic tendency. More details on the optimal $N \div n(h)$ relation may be found in [45, 11].

Furthermore, convergence graphs of all components of shear stress (4.3), in a respective relative error norm (4.7), calculated at the same nodes, are shown in Fig. 4c, d. Very good results may be observed for the primary solution (the Prandtl function). Results for derivatives (shear stress) are less accurate, though reasonable. It has to be stressed that no a-priori convergence estimation formulas for derivatives exist, for Monte Carlo methods and with respect to N . However, as it has been reported for FD [1] and meshless methods [6, 8], numerical FD derivatives are unconditionally super-convergent, namely their convergence rate, with respect to the (average) mesh size, is the same, or larger than the corresponding convergence of the primary solution.

Eventually, the MC formula was applied to the entire cloud of nodes, producing solution and derivatives values at all nodes. The fixed number of $N = 1000$ was used. This number may be justified twofold. First of all, it guarantees the total solution error below the 3% (see Fig. 4a, b and Fig. 11a in which a series of over one dozen MC trials were performed for the same N , thus producing the upper and lower bounds as well as the mean total error, limited by the 3% assumed error level). Furthermore, the assumed N may be interpreted as the estimation of the optimal regularization parameter, determined for the theoretical and experimental L-curves [56], built upon MC solutions. Such a parameter guarantees the optimal balance between the N and the solution error, namely the lowest solution error obtained for the lowest number of N .

Results (graphs of Prandtl function F and average shear stress τ) are presented in Fig. 5. They are comparable with results obtained by means of FDM [22, 11], though, as study of computational time indicates, the MC method becomes less effective for the larger number of unknown solution values.

5. Stationary heat flow analysis for anisotropic materials

5.1. Problem formulation

The following 2D stationary (time-independent) heat flow analysis problem is considered (see Fig. 7), namely: find such a C^2 temperature function $T : (x_1, x_2) \in \Omega \subset \mathfrak{R}^2 \rightarrow \mathfrak{R}$ that fulfills the following the Poisson (elliptic) differential equation for an anisotropic material

$$(5.1) \quad -\frac{\partial}{\partial x_1} \left(\lambda_1(x_1, x_2) \frac{\partial T}{\partial x_1}(x_1, x_2) \right) - \frac{\partial}{\partial x_2} \left(\lambda_2(x_1, x_2) \frac{\partial T}{\partial x_2}(x_1, x_2) \right) = f(x_1, x_2) \quad \text{in } \Omega$$

with the appropriate boundary conditions of essential (Dirichlet) type

$$(5.2) \quad T(x_1, x_2) = \bar{T}(x_1, x_2) \quad \text{on } \partial\Omega_e$$

and natural (Neumann) type

$$(5.3) \quad \lambda_n(x_1, x_2) \frac{\partial T}{\partial n}(x_1, x_2) = \bar{q}(x_1, x_2) \quad \text{on } \partial\Omega_n$$

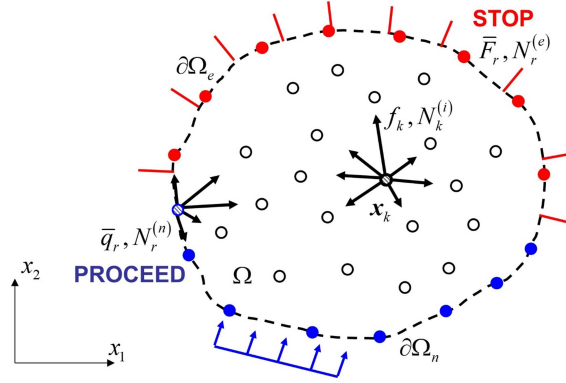


FIG. 7. Cloud of nodes with configuration of nodes (MFD star) for a meshless random walk, for the direct heat problem.

The following variables are introduced, namely

- $\lambda_1 = \lambda_1(x_1, x_2)$ – variable positive conductivity coefficient in x direction [J/(m · s · °C)],
- $\lambda_2 = \lambda_2(x_1, x_2)$ – variable positive conductivity coefficient in y direction [J/(m · s · °C)],
- $f = f(x_1, x_2)$ – intensity of heat generation inside the domain Ω , [J/(m³·s)],
- $\bar{T} = \bar{T}(x_1, x_2)$ – known temperature, ascribed to $\partial\Omega_e$, [°C],
- $\lambda_n = \lambda_n(x_1, x_2)$ – variable conductivity coefficient in a normal direction, outward to boundary,
- $\bar{q} = \bar{q}(x_1, x_2)$ – known heat flux, in a normal direction (represented by a versor $\mathbf{n} = [n_1, n_2]$) to $\partial\Omega_n$, [J/(m² · s)].

Similarly as in the torsion problem, the primary temperature function may be differentiated yielding components of the heat flux vector $\mathbf{q} = [q_1, q_2]$ and the total average flux q , namely

$$(5.4) \quad q_1 = -\lambda_1 \frac{\partial T}{\partial x_1}, \quad q_2 = -\lambda_2 \frac{\partial T}{\partial x_2}, \quad q = \sqrt{q_1^2 + q_2^2}.$$

Arguments (x_1, x_2) of T , λ_1 and λ_2 functions were omitted, for the sake of simplicity.

5.2. Computational model

Function values at all $n^{(i)}$ internal nodes \mathbf{x}_k as well as at all $n^{(n)}$ nodes \mathbf{x}_r located on $\partial\Omega_n$, constitute the set of $n^{(i)} + n^{(n)}$ unknowns. The star configurations \mathbf{S}_k and \mathbf{S}_r as well as difference coefficient matrices \mathbf{M}_k and \mathbf{M}_r have to be determined in a standard manner. However, in order to apply the difference approximation schemes (3.7) and (3.6) to (5.1) and (5.3), respectively, the equation

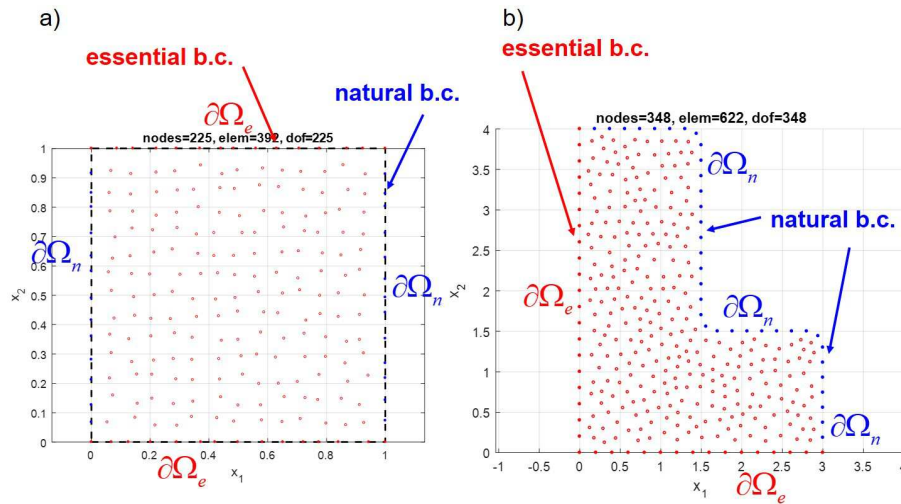


FIG. 8. Domains applied for a direct heat problem a) rectangular cross-section, b) L-Shape cross-section, with irregular distribution of nodes.

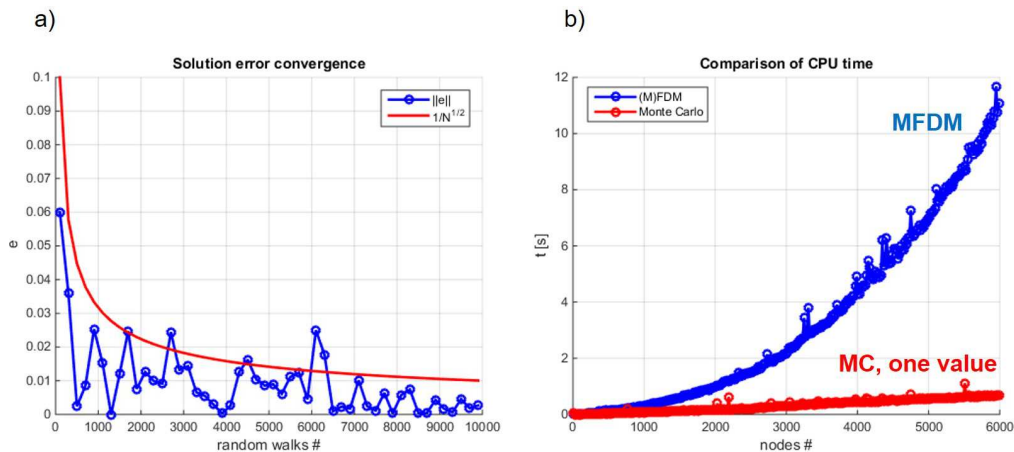


FIG. 9. Results for L-shape: results of N -convergence test (a) and comparison of computational time with respect to the number of nodes, for MFDM and MC methods (b).

(5.1) has to be modified to the following form

$$(5.5) \quad -\frac{\partial \lambda_1}{\partial x_1} \frac{\partial T}{\partial x_1} - \lambda_1 \frac{\partial^2 T}{\partial x_1^2} - \frac{\partial \lambda_2}{\partial x_2} \frac{\partial T}{\partial x_2} - \lambda_2 \frac{\partial^2 T}{\partial x_2^2} = f.$$

Derivatives of λ_1 and λ_2 may be evaluated analytically (assuming λ_1 and λ_2 are differentiable functions) or numerically (in case material parameters are defined by a discrete set). Collocation technique applied to (5.5) at $\mathbf{x}_k \in \Omega$ and (5.3) at $\mathbf{x}_r \in \partial\Omega_n$ yields the following relations

$$(5.6) \quad \begin{cases} T_k = \sum_{j=1}^m p_j T_{j(k)} \\ \frac{f_k}{\frac{\partial \lambda_1}{\partial x_1} \Big|_k M_{k2,0} + \lambda_1|_k M_{k4,0} + \frac{\partial \lambda_2}{\partial x_2} \Big|_k M_{k3,0} + \lambda_2|_k M_{k6,0}}, & \mathbf{x}_k \in \Omega, \\ T_r = \sum_{j=1}^m p_j T_{j(r)} + \frac{\bar{q}_r}{\lambda_1|_r n_1|_r M_{r2,0} + \lambda_2|_r n_2|_r M_{r3,0}}, & \mathbf{x}_r \in \partial\Omega_n, \end{cases}$$

in which

$$\begin{aligned} f_k &= f(\mathbf{x}_k), & \bar{q}_r &= \bar{q}(\mathbf{x}_r), & \lambda_1|_r &= \lambda_1(\mathbf{x}_r), & \lambda_2|_r &= \lambda_2(\mathbf{x}_r), & \lambda_1|_k &= \lambda_1(\mathbf{x}_k), \\ & & & & \lambda_2|_k &= \lambda_2(\mathbf{x}_k), & \frac{\partial \lambda_1}{\partial x_1} \Big|_k &= \frac{\partial \lambda_1}{\partial x_1}(\mathbf{x}_k), \\ \frac{\partial \lambda_2}{\partial x_2} \Big|_k &= \frac{\partial \lambda_2}{\partial x_2}(\mathbf{x}_k), & n_1|_r &= n_1(\mathbf{x}_r), & n_2|_r &= n_2(\mathbf{x}_r), & \mathbf{n} &= [n_1, n_2] \end{aligned}$$

is the versor normal to the boundary $\partial\Omega_n$. Selection probabilities are defined as

$$(5.7) \quad p_j = \begin{cases} \frac{\frac{\partial \lambda_1}{\partial x_1} \Big|_k M_{k2,j} + \lambda_1|_k M_{k4,j} + \frac{\partial \lambda_2}{\partial x_2} \Big|_k M_{k3,j} + \lambda_2|_k M_{k6,j}}{\frac{\partial \lambda_1}{\partial x_1} \Big|_k M_{k2,0} + \lambda_1|_k M_{k4,0} + \frac{\partial \lambda_2}{\partial x_2} \Big|_k M_{k3,0} + \lambda_2|_k M_{k6,0}}, & \mathbf{x}_k \in \Omega, \\ \frac{\lambda_1|_r n_1|_r M_{r2,j} + \lambda_2|_r n_2|_r M_{r3,j}}{\lambda_1|_r n_1|_r M_{r2,0} + \lambda_2|_r n_2|_r M_{r3,0}}, & \mathbf{x}_r \in \partial\Omega_n, \end{cases}$$

$j = 1, 2, \dots, m$, whereas the final Monte Carlo formula is given in the following explicit form

$$(5.8) \quad \left\{ \begin{array}{l} T_k \approx \frac{1}{N} \sum_r^{n^{(e)}} \bar{T}_r N_r^{(e)} \\ - \frac{1}{N} \sum_k^{n^{(i)}} \frac{f_k N_k^{(i)}}{\frac{\partial \lambda_1}{\partial x_1} \Big|_k M_{k2,0} + \lambda_1|_k M_{k4,0} + \frac{\partial \lambda_2}{\partial x_2} \Big|_k M_{k3,0} + \lambda_2|_k M_{k6,0}} \\ + \frac{1}{N} \sum_r^{n^{(n)}} \frac{\bar{q}_r N_r^{(n)}}{\lambda_1|_r n_1|_r M_{r2,0} + \lambda_2|_r n_2|_r M_{r3,0}}, \quad k = 1, 2, \dots, n^{(i)} + n^{(n)}, \\ T_r = \bar{T}_r, \quad r = 1, 2, \dots, n^{(e)}. \end{array} \right.$$

It is worth noticing that each random walk may be terminated if a boundary node located on $\partial\Omega_e$ is reached only. Consequently, the random walk proceeds for any other node (Fig. 7), taking the boundary ($N_r^{(e)}$ and $N_r^{(n)}$) as well as internal ($N_k^{(i)}$) indications (hits) into account. Similarly as in the torsion problem, the final Monte Carlo formula for an anisotropic thermal problem (5.8) is strongly affected by both discretization/approximation and stochastic types of errors. Therefore, a density of clouds of nodes has to be selected in an appropriate manner, resulting in an average modulus $h \ll 1$.

5.3. Numerical examples

The same domain geometries were considered, namely the rectangular and L-shaped ones, though with boundary conditions of both essential and natural types. Moreover, denser irregular nodes discretization models were used, with $n = 225$ and $n = 348$, respectively (Fig. 8). The thermal load functions (\bar{T}, f, \bar{q}) were manufactured on the basis of the analytical solution

$$(5.9) \quad \bar{T} = \sin\left(\frac{\pi x_1}{2} + \frac{\pi x_2}{2}\right)$$

as well as material functions $\lambda_1 = x_1^2$ and $\lambda_2 = x_2^2$. The first key issue, investigated here, is the distinction between the discretization and stochastic error types as well as their influence on the total solution error. Comparative computations were performed for the L-shape domain, for two clouds, namely the coarse cloud with $n = 41$ nodes and an average modulus $h = 0.6$ as well as the finer cloud with $n = 348$ nodes (Fig. 8). Results (i.e., relative true MC solution error $e_{true}^{MC} = \left| \frac{T_{MC} - T_{true}}{T_{true}} \right|$ and relative estimated MC solution error

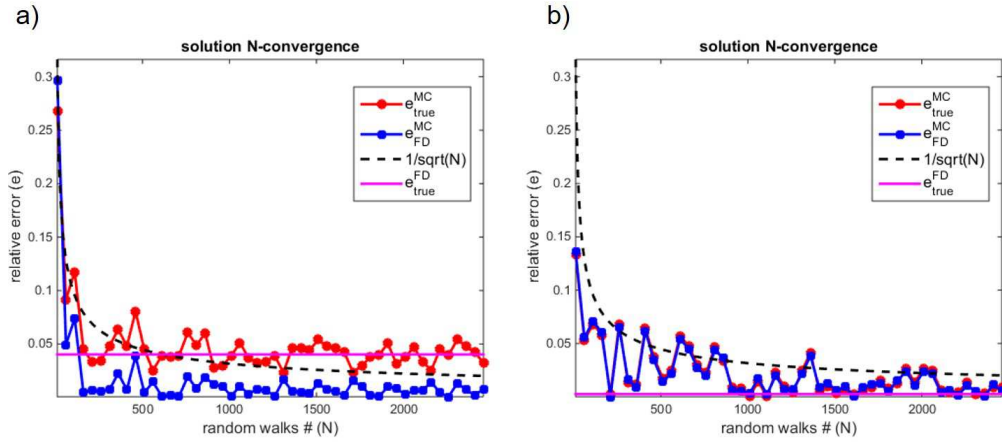


FIG. 10. Results of a N-convergence analysis for L-shape domain: a) coarse cloud with 41 nodes, b) fine cloud with 384 nodes.

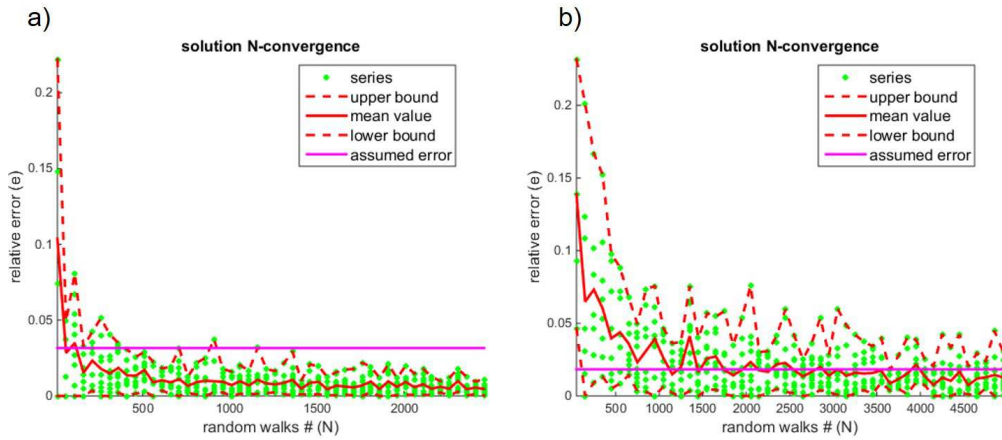


FIG. 11. Results of a N-convergence analysis of series of trials, for the L-shape domain and a) torsion problem with 3% of assumed solution error, b) thermal problem with 1% of assumed solution error.

$$e_{FD}^{MC} = \left| \frac{T_{MC} - T_{FD}}{T_{FD}} \right|$$
 in terms of N , as well as relative true FD solution error

$$e_{true}^{FD} = \left| \frac{T_{FD} - T_{true}}{T_{true}} \right|$$
 , independent from N , where T_{true} is the true analytical solution, according to (5.9), T_{FD} is the FD solution and T_{MC} is the Monte Carlo solution) are presented in Fig. 10. In case a cloud of nodes is too coarse, the discretization error may be significantly greater than the stochastic one (Fig. 10a).

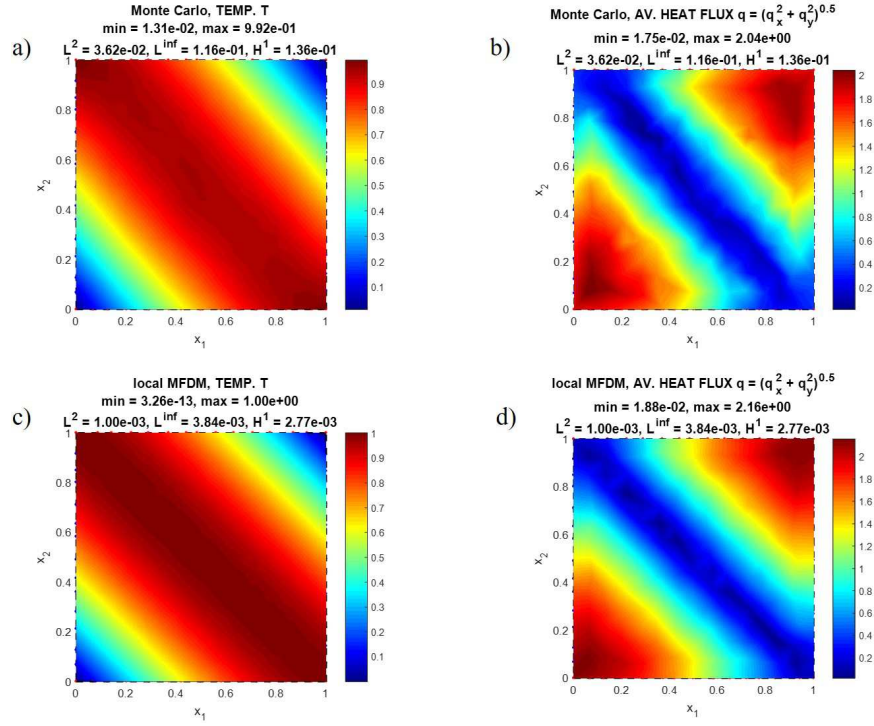


FIG. 12. Results of a stationary heat flow analysis for rectangular domain; a) Monte Carlo temperature, b) Monte Carlo average flux, c) FDM temperature, d) FDM average flux.

However, providing the cloud is fine enough, both errors produce very similar results (Fig. 10b).

Afterwards, N -convergence and computational time comparison tests were performed for L-shape, for one selected point $\mathbf{x}_k = [1.1309, 1.6472]$. Results are presented in Fig. 9. They are very similar to the ones obtained for the torsion problem, even though paths of random walks are longer and take more time to reach boundary edges with essential conditions. Since this is a more demanding problem (due to material anisotropy as well as mixed boundary conditions), $N = 3000$ random walks were assumed, thus limiting the total solution error at 1% level (Fig. 9a and Fig. 11b).

Moreover, the full analysis, for all nodes with unknown function values, was performed as well. Results are presented in Fig. 12 and Fig. 13, for both domains separately. The following graphs are included: Monte Carlo solutions for temperature and average heat flux (5.4) as well as equivalent FDM solutions. Additionally, true solution errors (with respect to the analytical one) were evaluated in L^2 , L^{inf} norms as well as H^1 semi-norm, and presented in figures' titles. Although Monte Carlo results are less precise and smooth, the overall so-

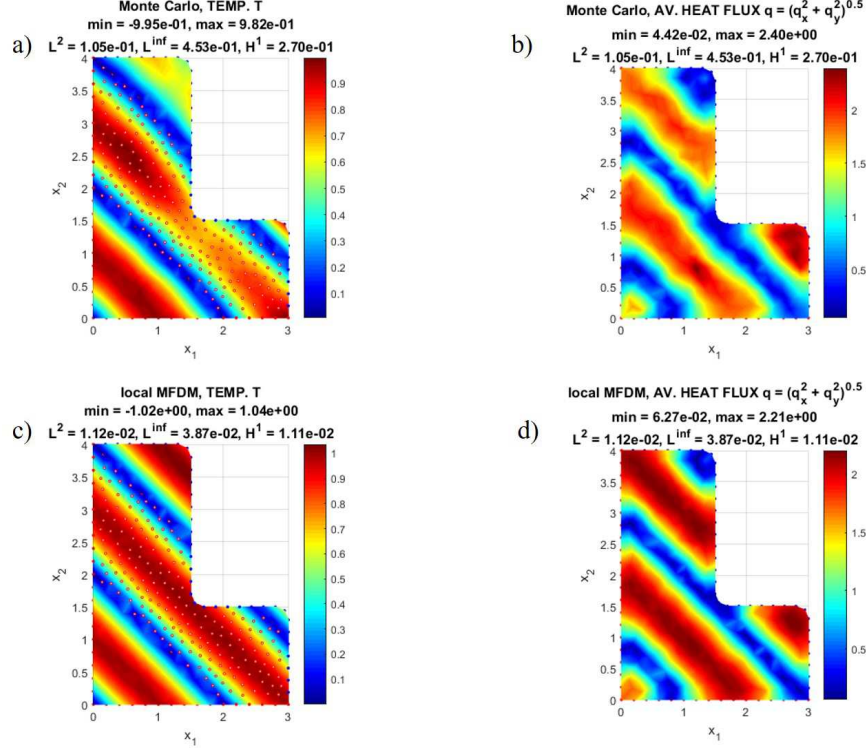


FIG. 13. Results of a stationary heat flow analysis for L-shape domain; a) Monte Carlo temperature, b) Monte Carlo average flux, c) FDM temperature, d) FDM average flux

lution quality is reasonable, especially when compared to the assumed analytical solution \bar{T} and corresponding FD solutions.

6. Physically non-linear heat problem

6.1. Problem formulation and computational model

The material with following thermal coefficients $\lambda_1 = \text{const}$ and $\lambda_2(T) = d \cdot T^2$ is assumed, where $d > 0$ [$\text{J}/(\text{m} \cdot \text{s} \cdot (\text{°C})^3)$] denotes a scalar coefficient, responsible for units unification. Additionally, let us assume boundary conditions of essential type only ($\partial\Omega = \partial\Omega_e$), for the sake of simplicity. Although a strong physical non-linearity appears, the problem remains elliptic, since $\lambda_2 > 0$ for all $\mathbf{x} \in \Omega$. The general local formulation (5.1) with (5.2) is considered, though (5.1) has a slightly modified form, namely

$$(6.1) \quad -\lambda_1 \frac{\partial^2 T}{\partial x_1^2} - \frac{\partial}{\partial x_2} \left(\lambda_2 \frac{\partial T}{\partial x_2} \right) = f.$$

After substitution of the assumed $\lambda_2 = \lambda_2(T)$ relation and execution of analytical differentiations, one obtains the following residual formula

$$(6.2) \quad R = -\lambda_1 \frac{\partial^2 T}{\partial x_1^2} - 2d \cdot T \left(\frac{\partial T}{\partial x_2} \right)^2 - d \cdot T^2 \frac{\partial^2 T}{\partial x_2^2} - f.$$

Afterwards, MWLS approximations (3.6) and (3.7) of partial derivatives of T are constructed, followed by the collocation technique at the internal node \mathbf{x}_k , leading to the difference version of residual error

$$(6.3) \quad R_k = -\lambda_1 (\mathbf{M}_k^{<4>} \mathbf{T}_k) - 2d \cdot T_k (\mathbf{M}_k^{<3>} \mathbf{T}_k)^2 - d \cdot T_k^2 (\mathbf{M}_k^{<6>} \mathbf{T}_k) - f_k.$$

The standard Newton–Raphson iterative procedure is applied

$$(6.4) \quad \mathbf{M}_k^{\mathbf{t}(l)} \cdot \Delta \mathbf{T}_k^{(l+1)} = -R_k^{(l)}$$

in which $\mathbf{M}_k^{\mathbf{t}(l)}$ is a $[1 \times (m+1)]$ tangent vector

$$(6.5) \quad \mathbf{M}_k^{\mathbf{t}(l)} = \frac{dR_k^{(l)}}{d\mathbf{T}_k^{(l)}} = -\lambda_1 \mathbf{M}_k^{<4>} - 4d \cdot T_k^{(l)} (\mathbf{M}_k^{<3>} \mathbf{T}_k^{(l)}) \mathbf{M}_k^{<3>} - d \cdot (T_k^{(l)})^2 \mathbf{M}_k^{<6>}$$

of difference coefficients, and $R_k^{(l)}$ is a scalar residual error

$$(6.6) \quad R_k^{(l)} = -\lambda_1 (\mathbf{M}_k^{<4>} \mathbf{T}_k^{(l)}) - 2d \cdot T_k^{(l)} (\mathbf{M}_k^{<3>} \mathbf{T}_k^{(l)})^2 - d \cdot (T_k^{(l)})^2 (\mathbf{M}_k^{<6>} \mathbf{T}_k^{(l)}) - f_k,$$

both evaluated at \mathbf{x}_k on every l -th iteration step ($l = 0, 1, \dots, l_{max}$, l_{max} – assumed maximum number of iterations) and

$$(6.7) \quad \Delta \mathbf{T}_k^{(l+1)} = \mathbf{T}_k^{(l+1)} - \mathbf{T}_k^{(l)}.$$

Calculations are performed until the estimated convergence error

$$(6.8) \quad \varepsilon^{(l+1)} = \frac{\|\Delta \mathbf{T}_k^{(l+1)}\|}{\|\mathbf{T}_k^{(l+1)}\|} \leq \varepsilon_{adm},$$

where ε_{adm} denotes the assumed admissible error, or $l = l_{max}$. Moreover, the initial solution $\mathbf{T}^{(0)}$ needs to be provided, corresponding to the linear problem (e.g., $\lambda_2 = \lambda_1$) and satisfying the non-homogeneous boundary conditions (5.2).

Selection probabilities assigned to an internal k -th node, of a move direction leading to one of its m neighbours (according to a cross criterion and meshless random walk principles), may be derived from (6.4), by the rearrangement of terms towards the evaluation of the central value $\Delta T_k^{(l)}$, namely

$$(6.9) \quad p_j = -\frac{M_{k_j}^{\mathbf{t}(l)}}{M_{k_0}^{\mathbf{t}(l)}}, \quad j = 1, 2, \dots, m.$$

Eventually, the final Monte Carlo formula for a solution increment at the particular node is as follows

$$(6.10) \quad \begin{cases} \Delta T_k^{(l)} \approx -\frac{1}{N} \sum_k^{n^{(i)}} \frac{R_k^{(l)} N_k^{(i)}}{M_{k_0}^{(l)}}, & \mathbf{x}_k \in \Omega, \quad k = 1, 2, \dots, n^{(i)}, \\ \Delta T_r^{(l)} = 0, & \mathbf{x}_r \in \partial\Omega, \quad r = 1, 2, \dots, n^{(e)}. \end{cases}$$

6.2. Numerical examples

Similar types of domain shapes, with discretizations and locations of selected internal points presented in Fig. 3, were applied. Additionally, the following data was assumed: $d = 1$ [$\text{J}/(\text{m} \cdot \text{s} \cdot \Delta(^{\circ}\text{C})^3)$], $\lambda_1 = 1$ [$\text{J}/(\text{m} \cdot \text{s} \cdot ^{\circ}\text{C})$], $l_{max} = 30$, $\varepsilon_{adm} = 10^{-6}$, $N = 3000$, as well as load parameters, corresponding to the analytical solution (5.9). The solution of a linear problem (i.e., for $\lambda_2 = 1$) was applied as the initial solution $\mathbf{T}^{(0)}$.

Results of the non-linear analysis by means of the meshless Monte Carlo approach are presented in Fig. 14. In Fig. 14a, c, convergence results are shown in the form of the Newton–Raphson error (6.8), for rectangle and L-shape domains, respectively. This error was evaluated in two, mean (blue lines) and maximum (red lines), norms, as well as for two types of solutions: primary Monte Carlo solution (solid lines) and reference FD solution (dotted lines). In Fig. 14b, d, graphs of the final solution (temperature) are shown, with solution norms and semi-norm indicated in graphs' titles. The following advantages of the MC method may be mentioned, namely possibility of solution of a non-linear problem in a linearized form for selected point(s) of the domain only with the same accuracy as for the MFDM method, simplicity of the final solution formula (6.10) in which boundary indications are determined only once, as well as shorter computational time (for rectangle: 15 seconds (MFDM) vs. 1 second (MC) and for L-shape: 36 seconds (MFDM) vs. 2 seconds (MC)).

7. Inverse heat problem

7.1. Problem formulation

Consider the stationary thermal problem (5.1) with (5.2) and (5.3), though with constant, material (λ_1, λ_2) as well as boundary load (\bar{T}, \bar{q}), parameters. Let us assume that some of these parameters are unknown and have to be determined on the basis of additional information, namely temperature measurements \hat{T}_i at M isolated internal points $\hat{\mathbf{x}}_i$

$$(7.1) \quad \hat{T}(\hat{\mathbf{x}}_i) = \hat{T}_i \pm \Delta T_i, \quad i = 1, 2, \dots, M$$

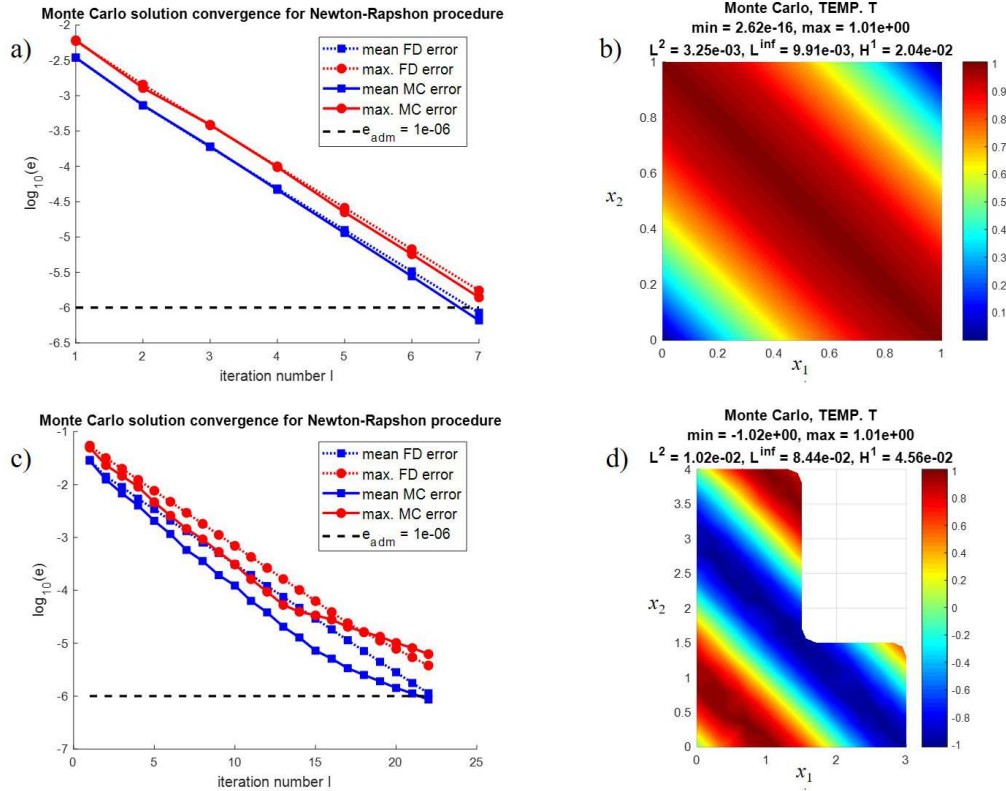


FIG. 14. Results of a physically non-linear heat flow analysis a) Newton–Raphson convergence for rectangle, b) the final temperature graph, for rectangle c) Newton–Raphson convergence for L-shape, d) the final temperature graph, for L-shape.

with assigned measurement tolerances ΔT_i each. This problem may be considered as the inverse heat problem (i.e., thermal load determination or/and material parameter identification). Its basic mathematical model constitutes the non-linear optimisation problem

$$(7.2) \quad (\lambda_1, \lambda_2, \bar{T}, \bar{q})^{(opt)} = \arg \min_{(\lambda_1, \lambda_2, \bar{T}, \bar{q})} J(\lambda_1, \lambda_2, \bar{T}, \bar{q}),$$

$$J = \sqrt{\frac{1}{M} \sum_{i=1}^M (T(\hat{\mathbf{x}}_i, \lambda_1, \lambda_2, \bar{T}, \bar{q}) - \hat{T}_i)^2}$$

with inequality constrains

$$(7.3) \quad |T(\hat{\mathbf{x}}_i, \lambda_1, \lambda_2, \bar{T}, \bar{q}) - \hat{T}_i| \leq \Delta T_i, \quad i = 1, 2, \dots, M,$$

based upon the mean square error between measured and evaluated temperature values. Variety of methods of deterministic, probabilistic and combined

types may be applied for solution of (7.2) with (7.3), for instance non-gradient searching methods (brute search method, genetic or evolutionary algorithms, see [14]) or gradient half-analytical methods (bisection, conjugate gradients, feasible directions, steepest descent method, see [2, 17]). However, regardless of the methods' type, numerical solution of the considered optimisation problem requires multiple solutions of auxiliary direct heat problems (5.1) with (5.2) and (5.3). Therefore, its computational complexity strongly depends on the selection of intermediate methods as well as the number of decision variables (here: unknown load and material parameters).

7.2. Computational model

Let us assume that the simple searching method (*brute search* approach) was applied in order to find optimal decision variables $(\lambda_1, \lambda_2, \bar{T}, \bar{q})^{(opt)}$, which minimize (7.2). Its main idea is based upon the assumption of admissible intervals for each decision variable (e.g., $\bar{T} \in [T_{min}, T_{max}]$). Afterwards, each interval is divided into a large number of subintervals which determine the intermediate sets of decision variables $(\lambda_1, \lambda_2, \bar{T}, \bar{q})$. For each set, the boundary value problem (5.1) with (5.2) and (5.3) is solved and the value of J is evaluated, according to (7.2). Eventually, the optimal set of variables is selected, for which J has the minimal value.

Standard deterministic methods (FEM, FDM, MFDM, BEM), applied for the solution of (5.1), produce values of the unknown temperature T , at all n nodes, even though they are required at a small number of measurement points M ($M \ll n$) in order to compare them with measured temperatures. Therefore, calculation time may grow rapidly, especially when one deals with a multidimensional optimisation problem (i.e., there are several decision variables). However, the Monte Carlo method allows for the effective elimination of this drawback. In fact, the final explicit formula (5.8) relates load and material parameters (unknown in inverse heat problems), with temperature value at the specified node. Therefore, temperature may be calculated at measurement locations only. Two approaches may be distinguished, namely

1. Application of the selected searching method and evaluation of nodal temperature values at M measurement points only, by means of the Monte Carlo formula (5.8), leading to J . Indication numbers $N_r^{(e)}$, $N_r^{(n)}$, $N_k^{(i)}$ are determined only once, for the entire process.
2. Direct analytical differentiation of J with respect to decision variables, which reduces to the differentiation of (5.8), thus leading to the necessary condition of the existence of the minimum of J , in the form of a small system of algebraic equations. Here, besides analytical tools (e.g., Lagrange multipliers), variety of gradient methods may be applied.

Moreover, flexible meshless discretization of the problem domain (by means of irregular cloud of nodes) may be adapted to measurement locations with no difficulties, since there is no imposed structure on it. For instance, generated nodes may be shifted to measurement locations, without any global modifications of the entire discretization.

7.3. Numerical examples

The considered problem domains (rectangle, L-shape), and the numbers of nodes are similar to those from previous examples, though modified were boundary values (Fig. 15a, c) as well as locations of four nodes in order to match four measuring locations exactly. Here, constant boundary values for temperature \bar{T} and heat flux \bar{q} were applied, instead of a given analytical solution. Selected boundary temperature values $\bar{T}_?$ are unknown (top value for rectangle as well as left and bottom values for L-shape) whereas other boundary temperature \bar{T} as well as remaining parameters ($\lambda_1 = \lambda_2 = 1 \text{ J}/(\text{m}\cdot\text{s}\cdot^\circ\text{C})$, \bar{q} , f) are fixed. The heat intensity function $f = x_1 - 2x_2 + 0.5$ was assumed. Temperature measurements are given at selected four locations ($M = 4$), shown in Fig. 15a, c. Those values were simulated on the basis of a FD numerical solution, obtained for one rank denser clouds of nodes and with $\bar{T} = -3^\circ\text{C}$ (for rectangle) and $\bar{T} = 0^\circ\text{C}$ (for L-shape). Moreover, a Gaussian noise was added to computed temperatures at nodes, with amplitude $\Delta\hat{T} = 0.5^\circ\text{C}$.

For both domains, calculations were performed by means of the brute search method (the first approach), combined with the Monte Carlo method with meshless random walk ($N = 1000$). Results – graphs of the target function, which 1000 values were evaluated inside the interval $\bar{T}_? \in [-10^\circ\text{C}, 10^\circ\text{C}]$ as well as the optimal solution $\bar{T}_?^{(opt)}$ – are presented in Fig. 15c, d, respectively. In both cases, very good accuracy was obtained, when comparing assumed original values ($\bar{T} = -3^\circ\text{C}$ and $\bar{T} = 0^\circ\text{C}$) with the recovered ones ($\bar{T}_?^{(opt)} = -2.965^\circ\text{C}$ and $\bar{T}_?^{(opt)} = 0.050^\circ\text{C}$). Moreover, these results were obtained within several seconds (in both cases), whereas the brute search method with traditional deterministic approach (here: MFDm) requires over a minute more (the solution of 1000 boundary value problems at all nodes is required). The advantages in reduction of computational time will be obviously clearer for multidimensional optimisation problems.

For the second approach, the direct differentiation of (7.2) with respect to $\bar{T}_?$ yields the following equation (the inverse of the square root, producing no roots, was neglected)

$$(7.4) \quad \min_{(\bar{T}_?)} J \iff \frac{dJ}{d\bar{T}_?} = 0 \rightarrow \frac{2}{M} \sum_{j=1}^M \left[(T_j(\bar{T}_?) - \hat{T}_j) \frac{1}{N} \sum_{r, \bar{T}=\bar{T}_?}^{n^{(e)}} N_{r(j)}^{(e)} \right] = 0,$$

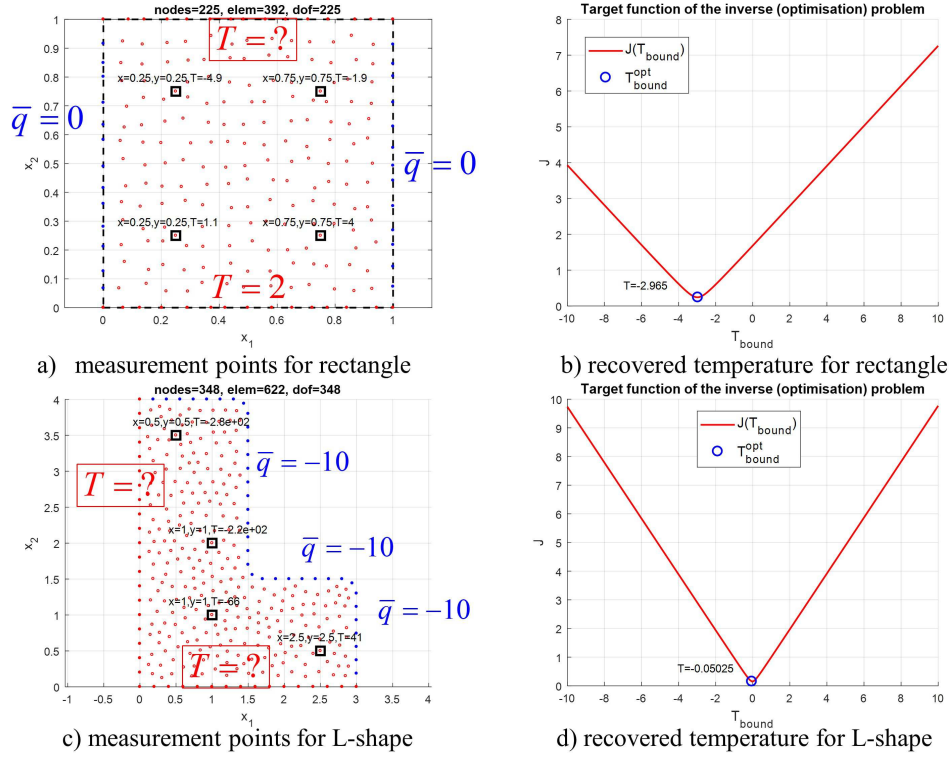


FIG. 15. Results of a stationary inverse heat flow analysis a) domain, nodes and measurements for rectangle, b) graph of a target function J , with optimal solution, for rectangle c) domain, nodes and measurements for L-shape, d) graph of a target function J , with optimal solution, for L-shape.

where $T_j(\bar{T}_?)$ are given by the Monte Carlo formula (5.8) (assuming constant material parameters $\lambda_1 = const$ and $\lambda_2 = const$). After substituting (5.8) into (7.4) and by simplifying and rearranging terms in the resulting equation, one may explicitly evaluate the unknown boundary temperature value $\bar{T}_?$, namely

$$(7.5) \quad \bar{T}_? \approx \frac{\sum_{j=1}^M \left(N \hat{T}_j - \sum_{r, \bar{T} \neq \bar{T}_?}^{n(e)} N_{r(j)}^{(e)} \bar{T}_r + \sum_k^{n(i)} c_k N_{k(j)}^{(i)} - \sum_r^{n(n)} c_r N_{r(j)}^{(n)} \right) \sum_{r, \bar{T} = \bar{T}_?}^{n(e)} N_{r(j)}^{(e)}}{\sum_{j=1}^M \left(\sum_{r, \bar{T} = \bar{T}_?}^{n(e)} N_{r(j)}^{(e)} \right)^2},$$

where

$$(7.6) \quad c_k = \frac{f_k}{\lambda_1|_k M_{k4,0} + \lambda_2|_k M_{k6,0}}, \quad c_r = \frac{\bar{q}_k}{\lambda_1|_r n_1|_r M_{r2,0} + \lambda_2|_r n_2|_r M_{r3,0}}.$$

Application of (7.5) to both examples yields the following results: $\bar{T}_7^{(opt)} = -3.125^\circ\text{C}$ for rectangle and $\bar{T}_7^{(opt)} = -0.110^\circ\text{C}$ for L-shape, which are fully competitive to those obtained by means of a brute search method, much more computationally expensive. Furthermore, the inverse heat problem was solved in a direct manner, by means of the explicit stochastic formula, yielding the unknown data parameter(s) on the basis of remaining load/material data as well as measurements, in the one-step algorithm. Therefore, this very simple example reflects the potential power of this approach, though the research is still in a preliminary stage and it is too early to draw more general conclusions.

8. Coupling meshless Monte Carlo with other computational methods

8.1. Problem formulation

Although the Monte Carlo method with random walk of meshless type may be considered as the combination of the standard Monte Carlo approach with meshless FDM, it may be additionally combined with other computational methods on various levels of a numerical analysis. Here, we focus on a method coupling in a domain divided into a set of disjoint subdomains, with a different method in each. For illustration purposes, let us assume that the entire problem domain Ω is divided into two subdomains Ω_1 and Ω_2 ($\Omega_1 \cup \Omega_2 = \Omega$ and $\Omega_1 \cap \Omega_2 = \emptyset$). This division is performed due to particular reasons, for instance Ω_1 is much more sensitive to thermal loading (e.g., due to stronger material conductivity) and therefore, requires a more accurate solution than the second, less important one Ω_2 . One may apply completely different methods in both subdomains, with independent discretization densities, approximation orders, non-conforming meshes and enforce solution continuity conditions on the mutual interface. The coupling idea is based upon the introduction of a very thin (though finite) material layer $\partial\Omega_{1,2}$, separating those two subdomains (Fig. 16). Its width z is selected according to appropriate heuristic assumptions and it depends on discretization and approximation parameters. Along this interface layer, an additional one-dimensional integral is evaluated. It results from a weak formulation (e.g., variational principle) of the original elliptic problem, posed in a local formulation. The reader is referred to [53, 55], for more detailed description of fundamentals of such a method coupling. Here, attention is laid upon the general formulation and the final system of algebraic equations.

For the sake of simplicity, let us assume that Ω_1 is discretized by the FEM, whereas the meshless Monte Carlo is applied for Ω_2 . Moreover, an isotropic material is assumed ($\lambda_1 = \lambda_2 = \lambda$). The local strong formulation of the elliptic boundary value problem for a heat transfer

$$(8.1) \quad -\lambda\Delta T = f$$

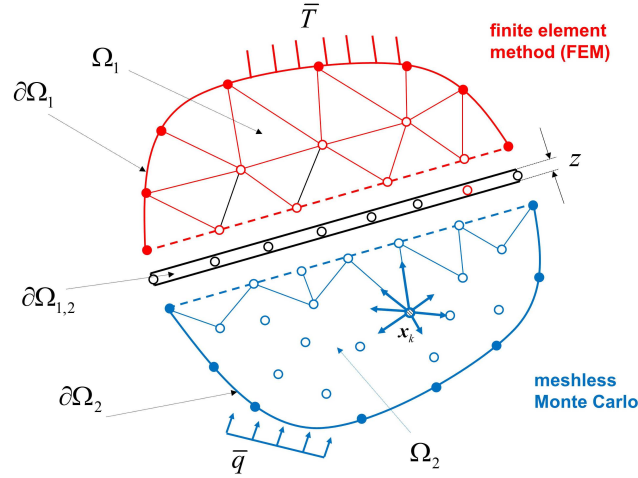


FIG. 16. The concept of coupling FEM with meshless Monte Carlo in one domain, divided into two disjoint subdomains.

with appropriate boundary conditions (5.2) and (5.3)), is a simplified form of (5.1), using global notation. The appropriate variational formulation has to be derived, starting from the global strong form

$$(8.2) \quad - \int_{\Omega} v \lambda \Delta T d\Omega = \int_{\Omega} v f d\Omega$$

in which all integrals may be decomposed into two subdomains and their mutual interface (assuming that $\int_{\Omega} = \int_{\partial\Omega_{1,2}} z$ on the interface subdomain $z\partial\Omega_{1,2}$), namely

$$(8.3) \quad - \int_{\Omega_1} v_1 \lambda \Delta T d\Omega - \int_{\Omega_2} v_2 \lambda \Delta T d\Omega - \int_{\partial\Omega_{1,2}} z v_{1,2} \Delta T d\partial\Omega \\ = \int_{\Omega_1} v_1 f d\Omega + \int_{\Omega_2} v_2 f d\Omega + \int_{\partial\Omega_{1,2}} z v_{1,2} f d\partial\Omega.$$

By integration by parts, the above equation may be reformulated into a global weak one (for Ω_1 and $z\partial\Omega_{1,2}$), with the additional boundary term on $\partial\Omega_1$ and a global strong one (for Ω_2) again, namely

$$(8.4) \quad - \int_{\partial\Omega_1} v_1 \mathbf{q} \cdot \mathbf{n} d\partial\Omega + \int_{\Omega_1} \nabla v_1 \cdot \mathbf{q} d\Omega - \int_{\Omega_2} \lambda v_2 \Delta T d\Omega + \int_{\partial\Omega_{1,2}} z \nabla v_{1,2} \cdot \mathbf{q} d\partial\Omega \\ = \int_{\Omega_1} v_1 f d\Omega + \int_{\Omega_2} v_2 f d\Omega + \int_{\partial\Omega_{1,2}} z v_{1,2} f d\partial\Omega$$

in which $T \in H_0^1 + \bar{T}$ is an unknown (trial) temperature function in Ω_1 , whereas $v_1, v_2, v_{1,2} \in H_0^1$ are test functions. Here, H_0^k is a Hilbert space of the k -th order, of functions which satisfy homogeneous boundary conditions on $\partial\Omega_e$ and \bar{T} is the affine transformation, required for the exact fulfillment of non-homogeneous boundary conditions for T on $\partial\Omega_e$. Additionally, $T \in H_0^2 + \bar{T}$ in Ω_2 . Although all functions and their derivatives remain continuous in (8.4), relevant approximated forms, appearing in integrals over an interface $\partial\Omega_{1,2}$, shall exhibit discontinuity. Therefore, two operators are introduced

$$(8.5) \quad \langle v \rangle_{1,2} = 0.5 \cdot (v_1 + v_2), \quad [[v]]_{1,2} = v_1 - v_2$$

allowing for an evaluation of a mean solution value at the interface. In this manner, one obtains the final variational formulation

$$(8.6) \quad \begin{aligned} & - \int_{\partial\Omega_1} v_1 \mathbf{q} \cdot \mathbf{n} \, d\partial\Omega + \int_{\Omega_1} \nabla v_1 \cdot \mathbf{q} \, d\Omega - \int_{\Omega_2} \lambda v_2 \Delta T \, d\Omega \\ & + \int_{\partial\Omega_{1,2}} \frac{\lambda}{z} [[v_{1,2}]] [[T]] \, d\partial\Omega + \int_{\partial\Omega_{1,2}} z \lambda \langle \nabla^T v_{1,2} \cdot \mathbf{s} \cdot \mathbf{s}^T \cdot \nabla T \rangle \, d\partial\Omega \\ & = \int_{\Omega_1} v_1 f \, d\Omega + \int_{\Omega_2} v_2 f \, d\Omega + \int_{\partial\Omega_{1,2}} z \langle v_{1,2} \rangle f \, d\partial\Omega, \end{aligned}$$

where $\mathbf{s} = [s_1, s_2]$ is a versor, tangent to the interface.

8.2. Computational model

It has been assumed that the standard FE framework is applied to Ω_1 (2D model) and $\partial\Omega_{1,2}$ (1D model). Therefore, both test $v_1, v_{1,2}$ and temperature T functions have to be approximated by means of the same basis (shape) functions \mathbf{N}_1 (according to the Bubnov–Galerkin approach), for instance $T = \mathbf{N}_1 \cdot \mathbf{T}_1$ and $\nabla T = \mathbf{B}_1 \cdot \mathbf{T}_1$, where $\mathbf{B}_1 = \nabla \mathbf{N}_1$ and \mathbf{T}_1 denotes the vector of nodal degrees of freedom (i.e., temperature values at nodes of Ω_1 , including $\partial\Omega_{1,2}$). However, for the Ω_2 , with the meshless Monte Carlo approach, a test function v_2 is assumed in the form of the Dirac delta pseudo-function ($v_2 = \delta$). Due to its selective property, it produces the original local formulation of the heat problem (8.1), for which the final Monte Carlo formula (5.8) may be directly applied, yielding a vector \mathbf{T}_2 of nodal degrees of freedom (temperature values at nodes of Ω_2 , including $\partial\Omega_{1,2}$). Standard shape functions \mathbf{N}_2 and their derivatives $\mathbf{B}_2 = \nabla \mathbf{N}_2$ are required for those finite elements from Ω_2 which edges are located on $\partial\Omega_{1,2}$. In other words, a partially structural mesh has to be generated in Ω_2 , near the interface (Fig. 16). Taking everything into account, the final system of algebraic

equations may be presented in the following manner

$$(8.7) \quad \begin{bmatrix} \mathbf{K}_{1,1} & \mathbf{K}_{1,2} \\ \mathbf{K}_{2,1} & \mathbf{K}_{2,2} \end{bmatrix} \begin{bmatrix} \mathbf{T}_1 \\ \mathbf{T}_2 \end{bmatrix} = \begin{bmatrix} \mathbf{F}_1 \\ \mathbf{F}_2 \end{bmatrix}$$

where matrices and vector are as follows

$$(8.8) \quad \begin{aligned} \mathbf{K}_{1,1} &= \int_{\Omega_1} \lambda \mathbf{B}_1^T \cdot \mathbf{B}_1 \, d\Omega + \int_{\partial\Omega_{1,2}} \frac{\lambda}{z} \mathbf{N}_1^T \cdot \mathbf{N}_1 \, d\partial\Omega \\ &\quad + \frac{1}{2} \int_{\partial\Omega_{1,2}} z \lambda \mathbf{B}_1^T \cdot \mathbf{s} \cdot \mathbf{s}^T \cdot \mathbf{B}_1 \, d\partial\Omega, \\ \mathbf{K}_{1,2} &= - \int_{\partial\Omega_{1,2}} \frac{\lambda}{z} \mathbf{N}_1^T \cdot \mathbf{N}_2 \, d\partial\Omega + \frac{1}{2} \int_{\partial\Omega_{1,2}} z \lambda \mathbf{B}_1^T \cdot \mathbf{s} \cdot \mathbf{s}^T \cdot \mathbf{B}_2 \, d\partial\Omega, \\ \mathbf{K}_{2,1} &= - \int_{\partial\Omega_{1,2}} \frac{\lambda}{z} \mathbf{N}_2^T \cdot \mathbf{N}_1 \, d\partial\Omega + \frac{1}{2} \int_{\partial\Omega_{1,2}} z \lambda \mathbf{B}_2^T \cdot \mathbf{s} \cdot \mathbf{s}^T \cdot \mathbf{B}_1 \, d\partial\Omega, \\ \mathbf{K}_{2,2} &= \lambda \mathbf{I} + \int_{\partial\Omega_{1,2}} \frac{\lambda}{z} \mathbf{N}_2^T \cdot \mathbf{N}_2 \, d\partial\Omega + \frac{1}{2} \int_{\partial\Omega_{1,2}} z \lambda \mathbf{B}_2^T \cdot \mathbf{s} \cdot \mathbf{s}^T \cdot \mathbf{B}_2 \, d\partial\Omega, \\ \mathbf{F}_1 &= \int_{\Omega_1} \mathbf{N}_1^T f \, d\Omega + \frac{1}{2} \int_{\partial\Omega_{1,2}} z \mathbf{N}_1^T f \, d\partial\Omega + \int_{\partial\Omega_{n_1}} \mathbf{N}_1^T \bar{q} \, d\partial\Omega, \\ \mathbf{F}_2 &= \lambda \mathbf{T}_2 + \frac{1}{2} \int_{\partial\Omega_{1,2}} z \mathbf{N}_2^T f \, d\partial\Omega, \end{aligned}$$

where components of vector \mathbf{T}_2 are evaluated according to (5.8).

8.3. Numerical examples

Geometrical and thermal data was assumed, similarly as in Sec. 5, though with constant material parameters $\lambda_1 = \lambda_2 = 1 \text{ J}/(\text{m} \cdot \text{s} \cdot ^\circ\text{C})$. Straight interface (horizontal and skew) lines were generated, thus dividing both domains into two subdomains. In each case, the upper subdomain is discretized by finite elements (triangles for rectangular domain, quadrangles for L-shape domain) with linear (rectangle) and parabolic (L-shape) shape functions. Simultaneously, the meshless Monte Carlo method was applied to the lower domain. Results are presented in Fig. 17. The additional norm was evaluated and displayed in figures' titles, namely the average difference between two solutions on the interface ($J^{L_2} = \|T_1 - T_2\|$). It may be observed that a discontinuity rank is on the same level as solution accuracy, at least.

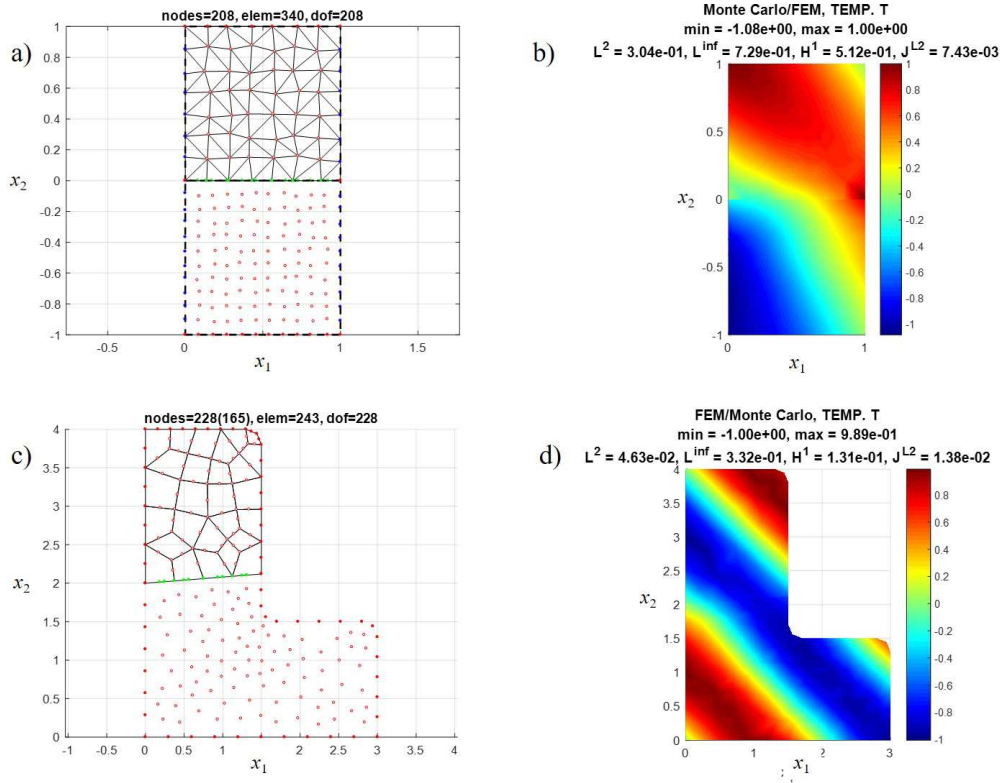


FIG. 17. Results of a method coupling: a) rectangle with interface and two independent discretization models, b) temperature for rectangle, c) L-shape with interface and two independent discretization models, d) temperature for L-shape.

9. Final remarks

The research presented in this paper is focused on the development of the meshless Monte Carlo (MC) method with the random walk (RW) technique and its application to selected scalar elliptic problems of mechanics and civil engineering. MC belongs to the wide class of probabilistic approaches and is commonly used in a variety of algebraic and differential problems. Its main concept is based upon the performance of series of simulations (trials) with an appropriately defined successful event. Eventually, the number of successful trials related to the total number of all trials, scaled by the dimension quantity may be treated as an unbiased estimator of the unknown solution to the considered problem. In this manner, MC combined with the appropriate RW technique, allows for a simple and effective estimation of the solution of the Laplace differential equation at selected point(s) of the domain. It does not require the time-consuming and computationally demanding generation and solution of a system of equation,

combining all unknown function values. The original concept, developed in this paper, is based upon the application of selected aspects of the meshless FDM to the MC/RW approach. Especially, classification criteria of nodes into FD stars as well as the MWLS approximation are taken into account. Therefore, an analysis of a wider class of problems, with more complex geometry, natural boundary conditions, non-homogeneous material and right-hand side functions as well as arbitrarily irregular clouds of nodes, is possible. The proposed MC with meshless RW approach was examined on selected 2D benchmark elliptic problems (torsion of a prismatic bar, stationary heat problem, non-linear heat problem as well as inverse heat problem), including possible coupling with other computational approaches in disjoint subdomains.

Further research includes, for instance, application of the meshless Monte Carlo random walk solution approach to analysis of the 3D elliptic equations, more complex inverse problems (in combination with genetic algorithms) as well as non-stationary thermo-mechanical problems. In case the reference problem has to be solved multiple times (e.g., within an incremental-iterative procedure or an implicit time integration scheme), series of random walks forming a net of nodal indications, are performed only once. Afterwards, the meshless Monte Carlo formula is applied to each solution increment, allowing for the significant reduction of the entire computational effort.

Acknowledgements

This research was supported by the National Science Centre, Poland, under the scientific project 2015/19/D/ST8/00816 (Computational coupled FEM / meshless FDM analysis dedicated to engineering non-stationary thermo-elastic and thermoplastic problems).

The substantial help from dr Roman Putanowicz, on the mesh generation stage, is highly appreciated and acknowledged.

References

1. J. ORKISZ, *Finite Difference Method (part III)*, Handbook of Computational Solid Mechanics, pp. 336–431, Springer, Berlin, 1998.
2. W.H. PRESS, S.A. TEUKOLSKY, W.T. VETTERLING, B.P. FLANNERY, *Numerical Recipes, The Art of Parallel Scientific Computing*, Cambridge University Press, Cambridge, 1999.
3. O.C. ZIENKIEWICZ, R.L. TAYLOR, *Finite Element Method Its Basis and Fundamentals*, Elsevier, London, 2005.
4. CH. CONSTANDA, D. DOTY, W. HAMILL, *Boundary Integral Equation Methods and Numerical Solutions: Thin Plates on an Elastic Foundation*, Springer, New York, 2016.

5. W.K. LIU, S. JUN, Y.F. ZHANG, *Reproducing kernel particle methods*, International Journal for Numerical Methods in Engineering, **20**, 1081–1106, 1995.
6. S. LI, W.K. LIU, *Meshfree and particle methods and their applications*, Applied Mechanics Review, **55**, 1–34, 2002.
7. G.R. LIU, *Mesh Free Methods: Moving Beyond The Finite Element Method*, CRC Press, Boca Raton, 2003.
8. S. MILEWSKI, *Meshless finite difference method with higher order approximation – applications in mechanics*, Archives of Computational Methods in Engineering, **19**, 1, 1–49, 2012.
9. N. METROPOLIS, S. ULAM, *The Monte Carlo method*, Journal of the American Statistical Association, American Statistical Association, **44**, 247, 335–341, 1949.
10. R. ECKHARDT, S. ULAM, *John von Neumann, and the Monte Carlo method*, Los Alamos Science, Special Issue, **15**, 131–137, 1987.
11. S. MILEWSKI, *Combination of the meshless finite difference approach with the Monte Carlo random walk technique for solution of elliptic problems*, Computers & Mathematics with Applications, **76**, 4, 854–876, 2018.
12. B. MOLLER, M. BEER, *Fuzzy Randomness, Uncertainty in Civil Engineering and Computational Mechanics*, Springer, Berlin, 2004.
13. B.D. RIPLEY, *Pattern Recognition and Neural Networks*, Cambridge University Press, Cambridge, 2007.
14. D. GOLDBERG, *Genetic Algorithms in Search, Optimization and Machine Learning. Reading*, Addison-Wesley Professional, Boston, 1989.
15. R. CAZACU, L. GRAMA, *Steel truss optimization using Genetic Algorithms and FEA*, Procedia Technology, **12**, C, 339–346, 2014.
16. G. WANG, F. GUO, *A stochastic boundary element method for piezoelectric problems*, Engineering Analysis with Boundary Elements, **95**, 248–254, 2018.
17. S. MILEWSKI, *Determination of the truss static state by means of the combined FE/GA approach, on the basis of strain and displacement measurements*, Inverse Problems in Science and Engineering, **27**, 11, 1537–1558, 2019.
18. G.C. LUH, C.Y. WU, *Non-linear system identification using genetic algorithms, Proceedings of the Institution of Mechanical Engineers, Part I: Journal of Systems and Control Engineering*, **213**, 2, 105–118, 1999.
19. N. PERRONE, R. KAO, *A general finite difference method for arbitrary meshes*, Computers and Structures, **5**, 45–58, 1975.
20. M.J. WYATT, G. DAVIES, C. SNELL, *A new difference based finite element method*, Instn Engineers, **59**, 2, 395–409, 1975.
21. T. LISZKA, J. ORKISZ, *The finite difference method at arbitrary irregular grids and its application in applied mechanics*, Computers and Structures, **11**, 83–95, 1980.
22. S. MILEWSKI, *Selected computational aspects of the meshless finite difference method*, Numerical Algorithms, **63**, 1, 107–126, 2013.
23. M.D. DONSKER, M. KAC, *A sampling method for determining the lowest eigenvalue and the principle eigenfunction of Schrödinger's equation*, Journal of Research of the National Bureau of Standards, **44**, 551–557, 1951.

24. G.E. FORSYTHE, R.A. LEIBLER, *Matrix inversion by a Monte Carlo method*, Mathematical Tables and Other Aids to Computation, **4**, 127–129, 1950.
25. J.H. CURTISS, *Monte Carlo methods for the iteration of linear operators*, Journal of Mathematics and Physics, **32**, 209–232, 1953.
26. J.H. CURTISS, *A theoretical comparison of the efficiencies of two classical methods and a Monte Carlo method for computing one component of the solution of a set of linear algebraic equations*, Symposium on Monte Carlo Methods, H.A. Meyer [Ed.], Wiley, New York, pp. 191–233, 1956.
27. H. NIEDERREITER, *Quasi-Monte Carlo methods and pseudo-random numbers*, Bulletin of American Mathematical Society, **84**, 957–1041, 1978.
28. M. MASCAGNI, *High dimensional numerical integration and massively parallel computing*, Contemporary Mathematics, **1**, 115, 53–73, 1991.
29. M.E. MULLER, *Some continuous Monte Carlo methods for the Dirichlet problem*, Annals of Mathematical Statistics, **27**, 569–589, 1956.
30. J.F. REYNOLDS, *A Proof of the Random-Walk Method for Solving Laplace's Equation in 2-D*, The Mathematical Gazette, Mathematical Association, **49**, 370, 416–420, 1965.
31. S. HOSHINO, K. ICHIDA, *Solution of partial differential equations by a modified random walk*, Numerical Mathematics, **18**, 61–72, 1971.
32. A.S. SIPIN, *Solving first boundary value problem for elliptic equations by Monte Carlo method*, Monte Carlo Methods, Computational Mathematics and Mathematical Physics, **2**, 113–119, 1979.
33. T.E. BOOTH, *Exact Monte Carlo solutions of elliptic partial differential equations*, Journal of Computational Physics, **39**, 396–404, 1981.
34. A.F. GHONIEM, F. S. SHERMAN, *Grid-free simulation of diffusion using random walk methods*, Journal of Computational Physics, **61**, 1–37, 1985.
35. S.M. ERMAKOV, V.V. NEKRUTKIN, A.S. SIPIN, *Random Processes for Classical Equations of Mathematical Physics*, Kluwer Academic Publishers, Dordrecht, 1989.
36. K.K. SABELFELD, *Monte Carlo Methods in Boundary Value Problems*, Springer, Berlin, Heidelberg, New York, 1991.
37. A. HAJI-SHEIKH, E.M. SPARROW, *The floating random walk and its application to Monte Carlo solutions of heat equations*, SIAM Journal on Applied Mathematics, **14**, 2, 370–389, 1966.
38. I. DIMOV, O. TONEV, *Random walk on distant mesh points Monte Carlo Methods*, Journal of Statistical Physics, **70**, 1993.
39. G.A. MIKHAILOV, *New Monte Carlo Methods With Estimating Derivatives*, V. S. P. Publishers, Boston, 1995.
40. M.N. SADIKU, *Monte Carlo Methods for Electromagnetics*, Taylor, London, 2009.
41. W. YU, X. WANG, *Advanced Field-Solver Techniques for RC Extraction of Integrated Circuits*, Springer, Berlin, 2014.
42. S. TALEBI, K. GHAREHBASH, H.R. JALALI, *Study on random walk and its application to solution of heat conduction equation by Monte Carlo method*, Progress in Nuclear Energy, **96**, 18–35, 2017.

43. A. JURLEWICZ, P. KERN, M.M. MEERSCHAERT, H.-P. SCHEFFLER, *Fractional governing equations for coupled random walks*, *Computers and Mathematics with Applications*, **64**, 10, 3021–3036, 2012.
44. C.N. ANGSTMANN, B.I. HENRY, I. ORTEGA-PIWONKA, *Generalized master equations and fractional Fokker–Planck equations from continuous time random walks with arbitrary initial conditions*, *Computers and Mathematics with Applications*, **73**, 6, 1315–1324, 2017.
45. P. RAMACHANDRAN, M. RAMAKRISHNA, S.C. RAJAN, *Efficient random walks in the presence of complex two-dimensional geometries*, *Computers and Mathematics with Applications*, **53**, 2, 329–344, 2007.
46. K. SABELFELD, N. MOZARTOVA, *Sparsified randomization algorithms for large systems of linear equations and a new version of the random walk on boundary method*, *Monte Carlo Methods and Applications*, **15**, 3, 257–284, 2009.
47. G. MILSTEIN, M.V. TRETAKOV, *Stochastic Numerics for Mathematical Physics*, Springer, Berlin, 2010.
48. F. BERNAL, J.A. ACEBRON, *A comparison of higher-order weak numerical schemes for stopped stochastic differential equations*, *Communications in Computational Physics*, **20**, 703–732, 2016.
49. K. BACLAWSKI, M.D. DONSKER, M. KAC, *Probability, Number Theory, and Statistical Physics, Selected Papers*, The MIT Press, Cambridge, Massachusetts, pp. 268–280, 1979.
50. C.-O. HWANG, M. MASCAGNI, J.A. GIVEN, *A Feynman–Kac path-integral implementation for Poisson’s equation using an h -conditioned Green’s function*, *Mathematics and Computers in Simulation*, **62**, 3–6, 347–355, 2003.
51. P. LANCASTER, K. SALKAUSKAS, *Surfaces generated by moving least-squares method*, *Mathematics of Computation*, **155**, 37, 141–158, 1981.
52. P. LANCASTER, K. SALKAUSKAS, *Curve and Surface Fitting*, Academic Press Inc., London, 1990.
53. J. JAŚKOWIEC, S. MILEWSKI, *The effective interface approach for coupling of the FE and meshless FD methods and applying essential boundary conditions*, *Computers and Mathematics with Applications*, **70**, 5, 962–979, 2015.
54. S. MILEWSKI, R. PUTANOWICZ, *Higher order meshless schemes applied to the finite element method in elliptic problems*, *Computers & Mathematics with Applications*, **77**, 3, 779–802, 2019.
55. J. JAŚKOWIEC, S. MILEWSKI, *Coupling finite element method with meshless finite difference method in thermomechanical problems*, *Computers and Mathematics with Applications*, **72**, 9, 2259–2279, 2016.
56. P.C. HANSEN, *The L-Curve and its Use in the Numerical Treatment of Inverse Problems, Computational Inverse Problems*, [in:] *Electrocardiology, Advances in Computational Bioengineering*, WIT Press, Boston, pp. 119–142, 2000.

Received November 14, 2018; revised version September 14, 2019.

Published online October 25, 2019.

